Progress in Nuclear Magnetic Resonance Spectroscopy 144–145 (2024) 1–14

Contents lists available at ScienceDirect

Progress in Nuclear Magnetic Resonance Spectroscopy

journal homepage: www.elsevier.com/locate/pnmrs

Magnetic resonance elastography in a nutshell: Tomographic imaging of soft tissue viscoelasticity for detecting and staging disease with a focus on inflammation

Tom Meyer [a], Johannes Castelein [b,c], Jakob Schattenfroh [a], Anna Sophie Morr [a], Rafaela Vieira da Silva [d], Heiko Tzschätzsch [e], Rolf Reiter [a], Jing Guo [a], Ingolf Sack [a,*]

[a] Department of Radiology, Charité – Universitätsmedizin Berlin, Germany
[b] Department of Radiology & Nuclear Medicine and Molecular Imaging, University Medical Center Groningen, Netherlands
[c] Department for Biomedical Sciences, Faculty of Health and Medical Sciences, University of Copenhagen, Denmark
[d] Experimental and Clinical Research Center, a cooperation between the Max Delbrück Center for Molecular Medicine in the Helmholtz Association and Charité - Universitätsmedizin Berlin, Germany
[e] Institute of Medical Informatics, Charité – Universitätsmedizin Berlin, Germany

ARTICLE INFO

Edited by Steven Williams and David Neuhaus

Keywords:
Magnetic Resonance Elastography
MRE
Inflammation
Fibrosis
Brain
Liver

ABSTRACT

Magnetic resonance elastography (MRE) is an emerging clinical imaging modality for characterizing the viscoelastic properties of soft biological tissues. MRE shows great promise in the noninvasive diagnosis of various diseases, especially those associated with soft tissue changes involving the extracellular matrix, cell density, or fluid turnover including altered blood perfusion – all hallmarks of inflammation from early events to cancer development. This review covers the fundamental principles of measuring tissue viscoelasticity by MRE, which are based on the stimulation and encoding of shear waves and their conversion into parameter maps of mechanical properties by inverse problem solutions of the wave equation. Technical challenges posed by real-world biological tissue properties such as viscosity, heterogeneity, anisotropy, and nonlinear elastic behavior of tissues are discussed. Applications of MRE measurement in both humans and animal models are presented, with emphasis on the detection, characterization, and staging of diseases related to the cascade of biomechanical property changes from early to chronic inflammation in the liver and brain. Overall, MRE provides valuable insights into the biophysics of soft tissues for imaging-based detection and staging of inflammation-associated tissue changes.

1. Introduction

The mechanical properties of soft tissues play a critical role in the development and progression of disease [1,2]. For example, inflammation, a tissue response to injury, can be triggered by chronic mechanical friction, increased vascular pressure, or traumatic mechanical insults [3–6]. Inflammatory tissue itself exhibits altered mechanical properties resulting from a cascade of mechanically relevant processes. For instance, vascular leakage or immune cell infiltration – two hallmarks of inflammation – significantly alter coarse-grained mechanical tissue properties [7,8]. Beyond early inflammation, further downstream pathological processes such as matrix protein accumulation and crosslinking typically lead to tissue stiffening while tissue degeneration, atrophy, and necrosis cause softening. Therefore, many disease processes are associated with physical state transitions of the affected tissues over property ranges from soft to stiff and from elastic to viscous [9].

Although they originate at the microscopic level, the physical traits of tissues affect long-range interactions up to and including percolation, i.e., global or whole-organ properties [10]. The exceptional sensitivity of manual palpation to detecting lesions and tumors (derived from the Latin for swelling) stems from the fact that such abnormal formations are characterized by a hierarchy of crosslinks and adhesion points that

Abbreviations: EAE, experimental autoimmune encephalomyelitis; FE, finite elements; FoV, field of view; LFE, local frequency estimation; MASLD, Metabolic Dysfunction-associated Steatotic Liver Disease; MEG, motion encoding gradient; MRE, magnetic resonance elastography; MRI, magnetic resonance imaging; MS, multiple sclerosis; PNN, perineuronal nets; SWS, shear wave speed; t-FT, temporal Fourier transform; TR, repetition time; USE, ultrasound elastography.

* Corresponding author.
E-mail address: ingolf.sack@charite.de (I. Sack).

https://doi.org/10.1016/j.pnmrs.2024.05.002
Received 26 April 2024; Accepted 27 May 2024
Available online 29 May 2024

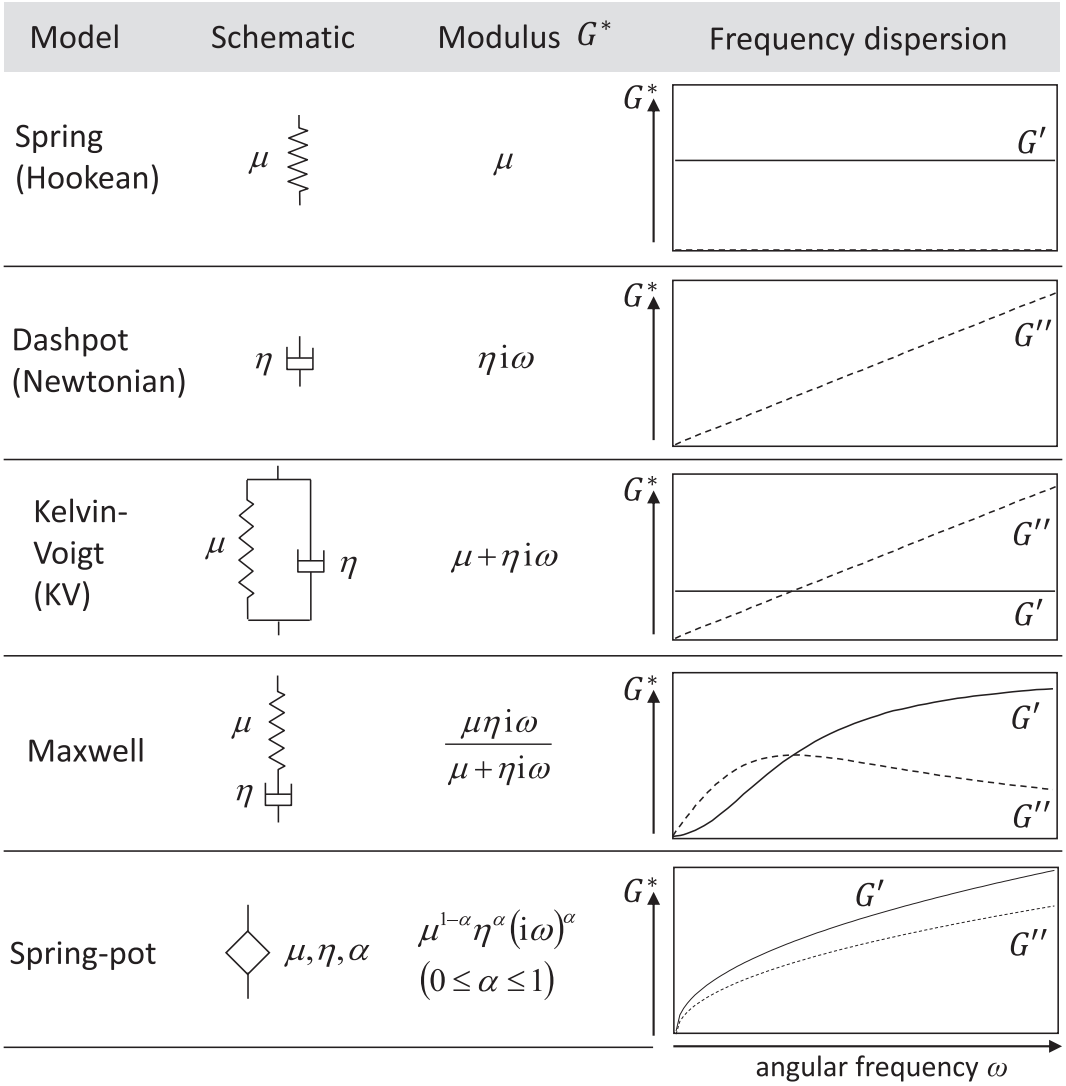

Fig. 1. Basic viscoelastic models that have been used to explain the dispersion of MRE-derived storage modulus G' and loss modulus G'' (similar functions can be drawn for shear wave speed and penetration rate). Dispersion in the context of MRE often refers to the changes in G' and G'' over frequency, which is a result of the tissue's intrinsic viscosity. While a spring models pure elastic behavior, a dashpot stands for a fluid that does not support shear waves and, consequently, cannot be assessed by MRE. Nevertheless, in combination with a spring, such as in the KV- or Maxwell model, the dashpot mimics the viscous loss encountered in soft biological tissues. The springpot is an interpolation between spring and dashpot with interpolation exponent α. While not supporting static stress, the springpot is the only two-parameter viscoelastic model that predicts a continuous increase in both G' and G'', as observed in most biological soft tissues.

add up to a macroscopic scaffold [11]. Even the physicians of Pharaoh Ahmose I used their fingers to detect disease, as described in the Ebers Papyrus of 1550 BCE [12]. Elastography was developed to give modern medical imaging modalities such as MRI and sonography the tactile senses to access the viscoelastic tissue properties that indicate disease [13].

Whereas ultrasound-based elastography (USE) is widely available, cost-effective, and can provide images in real-time [14], magnetic resonance elastography (MRE) maps soft tissue in three dimensions [15] and is considered the most accurate method for quantifying tissue viscoelasticity, particularly for the detection of liver fibrosis [16]. Therefore, MRE has significantly advanced our understanding of the in vivo biomechanical properties of tissues and their changes during disease progression. MRE and USE have been cross validated by simultaneous acquisitions in phantoms [17,18], liver [19,20] and brain [21] showing similar results whenever the same frequency range, inversion method and tissue region is considered.

MRE involves three key technical steps: (i) the stimulation of harmonic shear waves within the body, (ii) their encoding into the phase of the complex MRI signal, and (iii) the conversion of the resulting wave images into viscoelastic parameter maps [10]. The viscoelastic parameters that can be obtained include complex shear modulus, shear wave speed, wave attenuation, loss and storage properties, and model-based viscoelasticity [22].

Over the years, different techniques with complementary strengths and challenges have been developed. Upfront: there is no perfect single MRE technique that delivers what is theoretically possible given ideal imaging characteristics and tissue properties captured by our continuum mechanical models. In fact, biological tissue does not yield a single tone upon mechanical excitation but rather generates a full symphony of viscoelastic responses that overlap on a continuum of spatiotemporal scales. This is attributed to the hierarchical, heterogeneous, anisotropic, and nonlinear viscoelastic properties inherent to soft biological tissues. In addition, MRE is fundamentally slow, often taking minutes to acquire a complete data set, during which endogenous and stochastic motion occurs with amplitudes that exceed the induced harmonic deflections, while the intrinsic tissue properties can change.

Thus, MRE must be tailored to different clinical needs to make MRI

more quantitative, system-independent, and predictive. This article explains, in a nutshell, the basic concepts of MRE, introduces current approaches and validated techniques, and reviews clinical applications including their preclinical references with a focus on inflammatory processes.

2. Mechanical properties of soft biological tissue

2.1. Shear and compression modulus

Like any other mechanical test, MRE exploits Hooke's law, which describes the linear elastic deformation a material undergoes upon exposure to mechanical stresses [23]. In the simplest case, this deformation (strain) response is determined by a shear and compression modulus, both in units of kPa. While the shear modulus denotes the inherent resistance of a material to lateral deformation, meaning that the tissue volume does not change, the compression modulus is related to compression or dilation, i.e., changes in volume. Although it may seem academic to distinguish between shear and volumetric strain, their respective moduli are worlds apart. The compression modulus, in the range of gigapascals, is relatively uniform throughout the body, while the shear modulus varies by more than eight orders of magnitude and is in the range of tens to thousands of pascals in soft tissues [24]. Palpating fingers test the shear modulus by shifting tissue layers without volume changes for sensing the microarchitectural characteristics that are associated with disease. By contrast, the compression modulus is mainly determined by the tissue's high water content of 70 to 80 % evoking rather incompressible material properties. The situation is different at slower time scales when tissue fluid is allowed to be displaced or shifted during deformation [25]. At such scales, poroelastic effects provide sensitivity to blood perfusion and vascular pressure [26–28], illustrating the importance of excitation frequency in MRE. In a nutshell, higher stimulation frequencies probe solid-elastic properties, while shear waves at lower frequencies are influenced by elements that can permanently change position, such as fluids, motile cells, or vesicles [11].

2.2. Viscoelasticity

While strain energy is stored and re-stored in elastic materials, it is completely converted to kinetic energy and heat in fluids [29]. Thus, elastic solids and viscous fluids represent the two extremes of the spectrum of viscoelastic properties; between them, the recovery of shape after stress relaxation is delayed [12]. For harmonically oscillating stress, as in MRE, this delay causes a phase shift in the strain response that is proportional to the phase angle φ of the complex shear modulus $G^* = |G^*|\exp i\varphi$. G* can also be represented by its real part, storage modulus G', and its imaginary part, loss modulus G'', i.e., $G^* = G' + iG''$. The phase angle of the complex shear modulus, also called loss angle, is then obtained as $\varphi = \operatorname{atan} G''/G'$ [22]. An elastic solid has no loss modulus (G''=0) or loss angle ($\varphi = 0$) and does not exhibit frequency dispersion of G*=G', i.e., elasticity is constant over oscillation frequency. The opposite is true for pure fluids, which have no storage modulus (G'=0) and maximum loss angle ($\varphi = \pi/2$), giving rise to marked frequency dispersion of G*=G''. However, this hypothetical limit of maximum frequency dispersion with a loss angle of $\pi/2$ does not satisfy the wave equation because shear waves are not supported by fluids, rendering MRE unfeasible. Nevertheless, from solid G*=G' to fluid properties of G*=G'', G* becomes more and more dispersive, indicating increasing fluid material properties. Such a continuous transition from solid to fluid is nicely represented by an increase in loss angle φ from 0 to $\pi/2$ with $\pi/4$, indicating balanced solid–fluid properties [30]. Notably, φ as a measure of *tissue fluidity* increases with loss modulus G'' regardless of water content, while the fluidity of pure liquids is highest at zero viscosity. In essence, MRE is sensitive to elasticity through G' and viscosity either through G'' or φ. Because G* is a solid property, all MRE-derived parameters are related to the motility of particles and structures that transmit shear forces. Viscoelastic models are required to infer frequency-independent, intrinsic material parameters such as elasticity and viscosity from G', G'' or φ. The basic rheological models that relate two independent viscoelastic parameters to G* are the Kelvin-Voigt, the Maxwell, and the spring-pot model. Their representations assembled from basic spring and dashpot elements as well as dispersion functions are shown in Fig. 1. In biological soft tissues, most experiments have shown that G' and G'' increase with stimulation frequency [31,32]. These observations suggest that there is no independent material response of elasticity and viscosity, but rather an inherent mixture of the two, measured by MRE as viscoelasticity.

2.3. Shear waves

Remote palpation needs waves to transfer elastic energy deep into the tissue. While compression waves are polarized longitudinally with respect to their propagation direction, shear waves are transversely polarized. The first implies changes in density, which are associated with compression, the latter type of waves relates to shear modulus. Therefore, compression waves travel approximately 1000 times faster in soft biological tissue than shear waves (1500 m/s versus 1.5 m/s) [33]. As a result, at relatively low drive frequencies as used in MRE, compression waves have lengths on the order of 30 m and appear in MRE wave images without significant curvature while shorter shear waves of approximately 3 cm length are superimposed. The shear wave is the desired probe for remote palpation: the longer the shear wave, the higher the shear wave speed and corresponding shear modulus. Without viscoelastic dispersion, the shear wavenumber grows linearly with excitation frequency, making higher frequencies more favorable for wave analysis algorithms. However, it is a fundamental principle in acoustics that amplitude attenuation through viscous damping increases with wavenumber or excitation frequency. Therefore, the optimal range of excitation frequencies in MRE needs to be carefully balanced: on the one hand, wave analysis algorithms measure strain, i.e., the curvature of the waves, which should be sufficiently high relative to the achieved spatial resolution. On the other hand, the signal-to-noise ratio (SNR) of strain depends on total deflection amplitude [34], which decreases with frequency [35]. Therefore, MRE performed in clinical scanners balances the range of vibration frequencies between wave damping and shear strain, typically between 20 and 50 Hz for the brain [36], while most clinical studies investigating liver fibrosis are performed at 50 to 60 Hz [37]. Smaller and more heterogeneous organs such as the heart and prostate are typically investigated at higher frequencies of 60 to 150 Hz [38–40]. Notably, in the same way that viscoelastic damping impedes the use of higher frequencies, it supports low frequencies: according to the spring-pot viscoelastic model as shown in Fig. 1, tissue often behaves very soft at low excitation frequencies, giving rise to surprisingly short wavelengths even at extremely low excitation frequencies on the order of 10 Hz [41,42]. Adjusting wavelengths and strain SNR by increasing or decreasing excitation frequency makes MRE a multiscale method [43–45]. In small animals or tissue samples, higher vibration frequencies are required in order to squeeze several wave numbers into the smaller field of view [46–48]. Therefore, in the mouse brain, MRE operates in the kilohertz range, which provides higher shear modulus values than typically obtained in the range of clinical MRE, again due to the dispersion of the shear modulus [49]. Even when dispersion of shear modulus is ignored, relative conclusions in terms of *stiffer* or *softer* can be consistently drawn across the hierarchy of scales from the cell scale to coarse-grained in vivo properties measured by MRE [50,51].

3. Technical key points

3.1. Mechanical excitation of shear waves

MRE relies on continuous, time-harmonic vibrations, i.e., sinusoidal

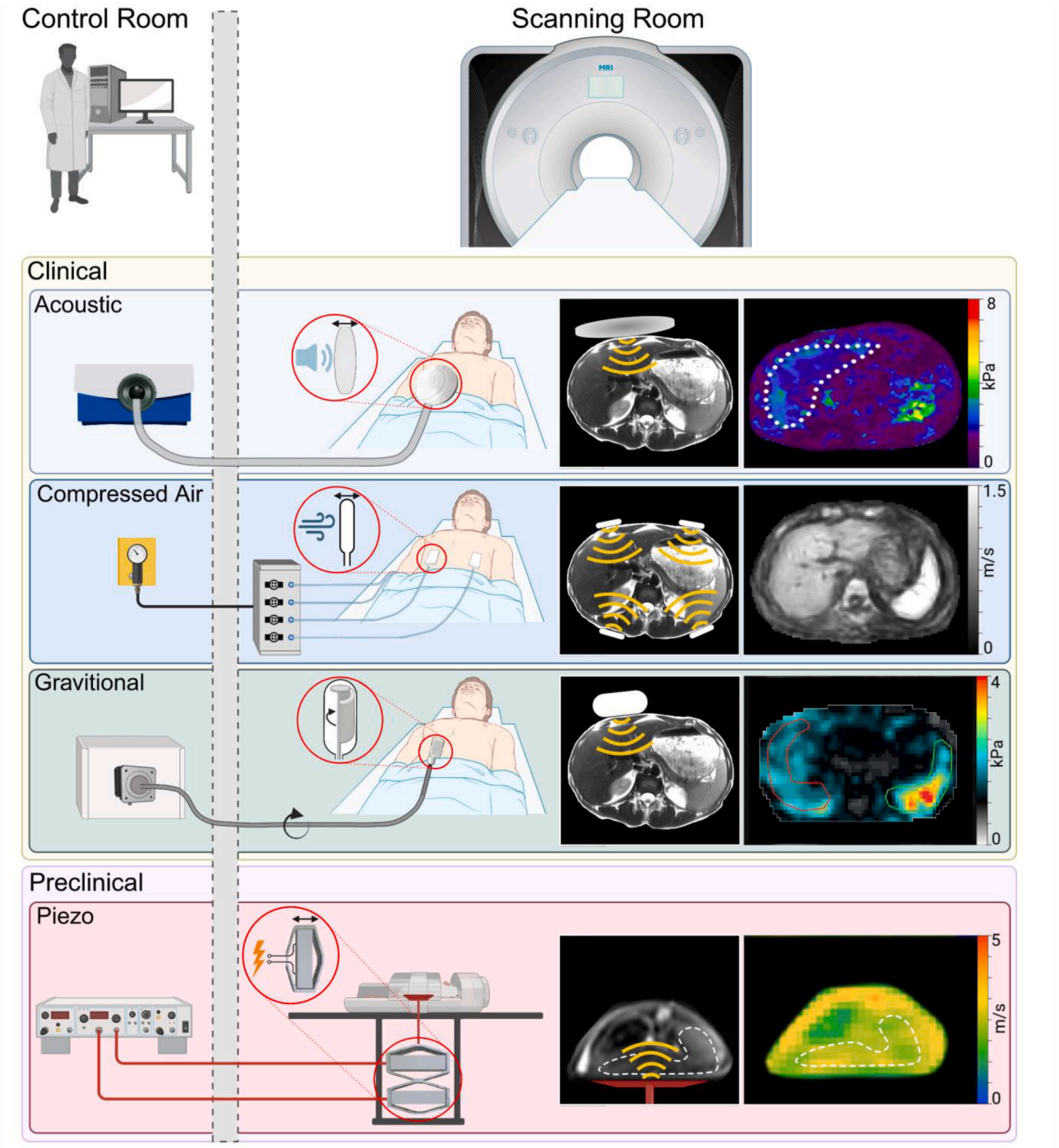

Fig. 2. Types of MRE vibration hardware used in clinical MRI scanners, including clinical and preclinical applications with resulting stiffness-related parameter maps. Three clinical driver systems are shown. They are based on an acoustic voice coil system [181], compressed air drivers [61], and a rotational eccentric mass driver [60]. The use of several drivers allows multidirectional wave excitation, supporting the generation of tomographic stiffness maps, as illustrated by the gray-scale shear wave speed image of human abdominal organs. Therefore, no organ-specific region is delineated. The experimental setup for preclinical applications is based on a piezoelectrical actuator, which can be driven at higher frequencies (300 to 800 Hz) than used in patients (20 to 80 Hz).

motion, in the frequency ranges mentioned above. This does not mean that MRE actuators have to perform strictly harmonic motion. MRE can also use transient impulses that are converted into harmonic motion within the tissue. As a natural protective mechanism, soft biological tissue attenuates high-strain shear waves and favors harmonic motion at the lowest (fundamental) frequency. Consequently, as the waves propagate through the tissue, the fundamental frequency of 1/TR increasingly dominates any periodic stimulation with repetition time TR. Typical TRs between consecutive RF excitations in MRI sequences are in the range of tens of milliseconds, resulting in frequencies <100 Hz when a mechanical pulse is applied at each TR [10].

Although there is flexibility in the way motion is induced, including various strategies such as scanner-intrinsic vibrations [52], piezoelectric actuators [53,54], Lorentz coils [55–57], loudspeakers [58,59], rotating masses [60], or compressed air pulses [61], MRE actuators should meet some important requirements: first, they should avoid magnetic field

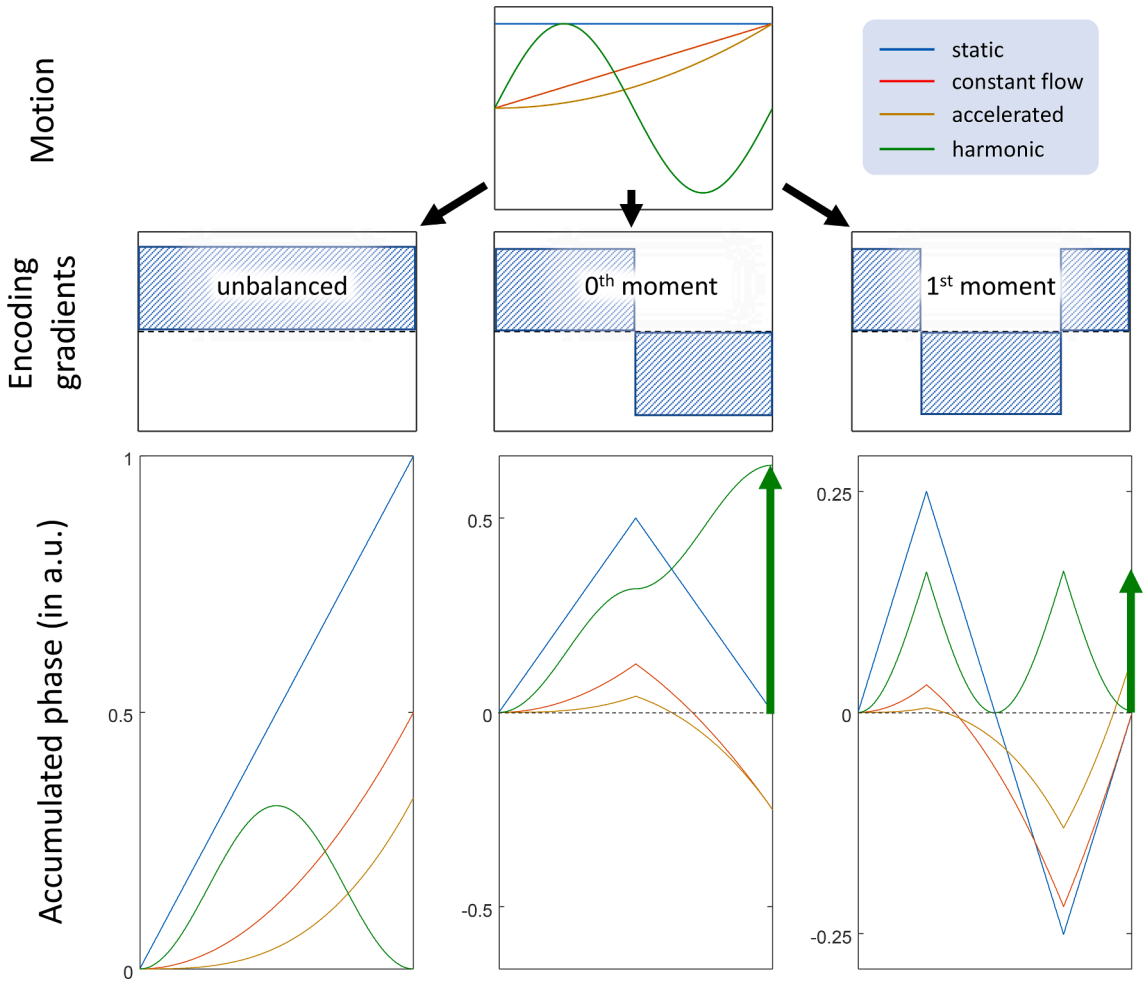

Fig. 3. Motion encoding in phase-contrast MRI, which requires encoding gradients, which in turn result in phase accumulation of the complex-valued MRI signal. As the encoding gradient is applied, static particles (blue lines) accumulate spin phase only with unbalanced gradients. In motion-sensitive PC-MRI, these spins are suppressed by using balanced gradients with 0th, 1st, or 2nd moment nulls, which suppress the spins of static, flowing (red lines), and accelerated (yellow lines) particles, respectively (2nd moment zero not shown). MRE is based on harmonic motion (green lines), whose maximum accumulated phase is indicated by green arrows.

interactions [62,63]. Nonmetallic actuators are preferred, while nonmagnetic actuators are mandatory for MRI safety. In addition, the timing of driver motion should be precisely controllable by the MRI sequence, either by resynchronizing each TR with trigger pulses or by locking the clock of the wave generator to the MRI [64]. While the first principle introduces slight phase distortions that interrupt the continuous flow of shear wave energy, the second principle requires a level of precision that is on the order of a μs per second of run time (e.g., 1 μs accumulates to 0.24 ms after 4 min of MRE scan time, which adds up to nearly 9° of phase shift for a 100 Hz vibration). Fig. 2 illustrates the current principles of MRE motion generation used in clinical MRI scanners for patient studies and preclinical research. Homogeneous delivery of vibration amplitudes to the region of interest is desirable to achieve sufficient strain SNR over the entire field of view (FoV). Full illumination of organs and tissues by shear waves is necessary for MRE to generate tomographic maps of mechanical properties across the full FoV. Therefore, use of several drivers placed around the region of interest, ideally combined with repeated acquisition at multiple frequencies, provides a wealth of mechanical information, regionally and dynamically, that stabilizes the inverse problem solutions as explained below [65].

3.2. Encoding shear waves by phase-contrast MRI sequences

Once shear waves have been induced in the tissue, the next step in MRE is to encode the resulting tissue deflections using phase-contrast MRI. In the presence of magnetic field gradients, the complex MRI signal is sensitive to motion. When the spins – the signal-emitting particles – move in a spatially varying magnetic field, their frequency changes slightly with their position within the field. This results in spins experiencing a net phase shift proportional to their displacement [66]. In this way, motion is *imprinted* on the phase of the complex MRI signal. In MRE, motion-encoding gradients (MEGs) are bipolar, mimicking a sine or cosine function over time to suppress the phase accrual of static and continuously moving spins, respectively [41]. Fig. 3 illustrates how the accumulated MRI phase increases over the time of the MEG with a spin motion that is zero, has constant velocity, is accelerated, or sinusoidal. It can be seen that the MEG acts as a finite difference operator in time and suppresses static phase shifts (zero moment nulling), flow (first moment nulling), or accelerating spins (second moment nulling). Consequently, the resulting phase images do not reflect true tissue deflections $u(t)$, but rather their first- or second-time derivative depending on the shape of the MEG, e.g., displacement velocity $\dot{u}(t)$ in flow MRI or phase-shifted oscillatory motion in MRE (first moment nulling: $\frac{dsin(t)}{dt} = \cos(t)$, second moment nulling: $\frac{d^2sin(t)}{dt^2} = -\sin(t)$). Since the MEG can be

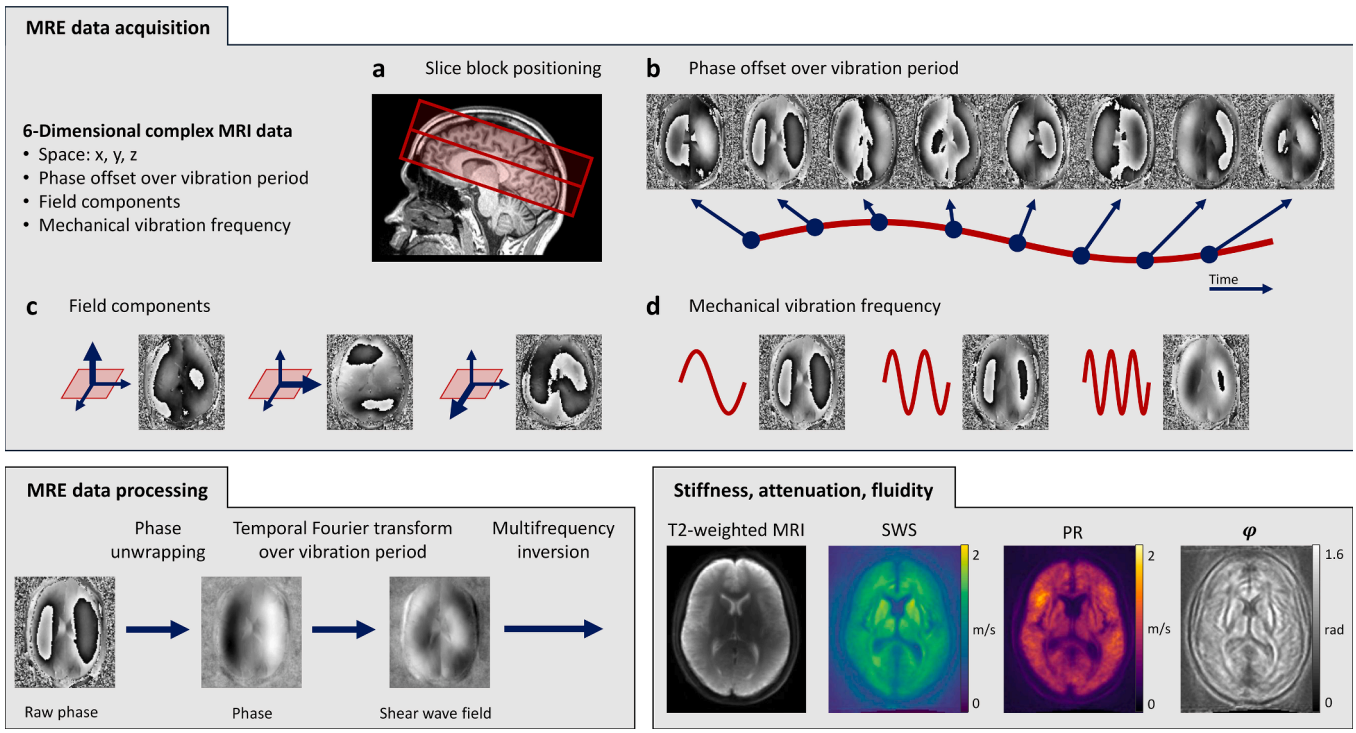

Fig. 4. Information pipeline in multifrequency MRE. Six-dimensional phase data are acquired for three spatial dimensions (a), phase variations over time (b), three field components (c), and multiple frequencies (d). MRE data processing includes phase unwrapping, temporal Fourier transform to separate the fundamental frequency, and multifrequency inversion. The MRE maps shown here were generated using phase-gradient-based multifrequency inversion (for shear wave speed, SWS, and penetration rate, PR), as explained in [182], or phase-angle-based direct inversion (for loss angle or fluidity φ), as explained in [74].

deployed along any Cartesian axis $i = \{x, y, z\}$, MRE has the unique ability to encode full 3D vector fields $u_i(t)$ [67]. Fig. 4 shows a set of raw MRE phase data representing the encoded motion at different time steps over one vibration period, in three orthogonal encoding directions, and at different frequencies.

3.3. Postprocessing of raw phase images in MRE

An MRE experiment typically consists of repeated encodings with shifted wave phase in order to capture motion $u_i(t)$ at N different time points over a vibration period. This allows extraction of fundamental frequency f from the phase images by performing a temporal Fourier transformation (t-FT) over N time points for each pixel. The generation of complex wave images $\widetilde{u}_i(f)$ is a key step in MRE postprocessing as it suppresses signals from other Fourier components such as induced by breathing [68]. Furthermore, t-FT collapses the relevant time information into a harmonic wave field that satisfies the complex wave equation [29]. In addition, complex wave images $\widetilde{u}_i(f)$ have a factor $\sqrt{N/2}$ higher SNR than raw data $u_i(t)$. However, t-FT is not the first step in MRE postprocessing as it must be applied to unwrapped phase images. Thus, elimination of aliased phases as shown in Fig. 4 requires unwrapping algorithms to be applied to noisy raw data, which still contain stochastic, nonharmonic, motion. Therefore, robust unwrapping algorithms have been developed, which deliver smooth phases but do not necessarily reflect the ground truth of wave phases in 3D and time. Physically correct unwrapped phases are often not easy to attain due to motion inconsistencies or rapid patient movements of only a few microns occurring between time points, field components, or adjacent image slices [69]. Stable unwrapping methods widely used in MRE include techniques based on 2D pathfinding, which, however, are sometimes disturbed at discontinuities [70] and Laplacian-operator-based methods, which generate smooth but sometimes biased wave fields [12]. To improve unwrapping, dual encoding strategies have been proposed, which basically combine raw phase images encoded with different gradient sensitivities to generate images that are widely wrap-free, however, at the expense of longer acquisition time [71,72]. In essence, MRE wave images should be high-dimensional to mitigate phase inconsistencies due to stochastic motion, phase jitter, inefficient encoding, or wave attenuation [69,73]. In fact, the overdetermination of MRE information by repeated acquisitions of wave phases, components and frequencies provides stability for efficient solutions to multidimensional unwrapping and wave inversion [74].

3.4. Wave inversion

The final step in MRE is the conversion of complex wave fields $\widetilde{u}_i(f)$ into parameter maps. Reconstruction of maps of shear modulus from harmonic wave fields requires solution of the inverse problem of time-harmonic waves [75,76]. In other words, wave inversion infers material properties from the curvature and attenuation of local displacements. Both the curvature and attenuation of a wave are determined by relative changes in local deflections on a spatial scale. Therefore, classical MRE reconstruction relies on the determination of spatial gradients, not absolute deflections. Mathematically, this is prescribed in the wave equation, a second-order partial differential equation that incorporates Laplacian field $\Delta\widetilde{u}_i(f)$. In its simplest form, the wave equation is a scalar equation with only one unknown, the shear modulus: $G^* = -\rho 2\pi f \widetilde{u}_i / \Delta\widetilde{u}_i$ (with ρ denoting mass density). However, to arrive at this simplification, known as direct Helmholtz inversion, one must make several assumptions which are hard to justify from a rigorous biomechanics perspective. These assumptions with their consequences in brackets are:

- Small strain (the MRE-induced deflection amplitudes satisfy the limit of linear elasticity of Hooke's law) [77]
- Isotropy (any direction dependence is ignored, reducing the number of independent elastic coefficients in Hooke's law from 21 to 2: one compression and one shear modulus) [78–82]

- Incompressibility, no compression wave, no pressure offset in $\widetilde{u}_i$ (all terms in the motion equation related to volumetric changes can be omitted) [83,84]
- Local homogeneity, viscoelastic properties change only shallowly, no distinct interfaces between tissues of different mechanical properties (constant G*, spatial derivatives of G* equal zero) [85–87]

Small strain seems to be a valid assumption given that strain amplitudes in MRE are on the order of 10^{-3} for shear waves and 10^{-4} for compression waves [88,89] as long as we ignore the fact that some tissue types, e.g., tumors or dilated lung and myocardium, are pre-strained [90–95]. Arguably, the other three assumptions listed above are likely to be invalid. Worse, the assumption of homogeneity, for example, calls into question the whole approach of generating parameter maps by MRE, since the very purpose of these maps is to represent exactly what is ignored here: the heterogeneity of viscoelasticity. Additionally, there are a few numerical challenges in solving the Helmholtz equation on the finite grid that represents the digital support for MRE wave images. First, numerical gradient operators have a finite size within which derivatives across boundaries are biased. Second, the digital support of waves is either too small or too large, causing overestimation of values – the discretization bias – or noise-related underestimation, respectively [96]. Only in a very narrow window of 8 to 12 pixels per wavelengths do discretization bias and noise effects cancel each other in MRE direct inversion [96,97]. To illustrate, the estimation of MRE is analogous to the attempt to quantify the slope of the local incline of individual steps on a staircase, where the height of each step may fluctuate to an unknown extent. The elastogram is then obtained by dividing the staircase by the noisy slopes. Obviously, careful denoising is needed here to extract meaningful information. Several robust denoising approaches have been reported in the literature, including bandpass filters of desired wavenumbers (k) in k-space [98], multidimensional derivative kernels of extended sizes in image space [99], wavelets [100], and forward model fitting by expanding MRE wave images into sets of harmonic base functions [85,101–103]. Artificial neural networks have also been trained to mitigate the noise curvature problem in MRE by patch-wise comparison of complex wave images with simulated superposition of traveling waves [104,105]. Nonetheless, the quest is still open for solutions that avoid a priori assumptions about wanted signal (shear waves in a predefined k-band) versus unwanted signal (low-k compression waves and high-k noise). It seems as if the wave equation takes its toll: second spatial derivatives suffer from noise, while variational approaches involve closed-path integration that again resembles a difference operator [85,86]. Forward solutions are computationally expensive and require knowledge of boundary conditions [12]. One way to trick the wave equation is based on its solution: Manduca et al. proposed to derive the phase gradient of a single k-wave (plane wave) [106]. The basic idea is that the phase of a complex plane wave accrues linearly along the propagation axis x. The slope of this wave phase is equal to the wavenumber k_x, which is retrieved as the x-derivative, i.e., the plane wave phase gradient. Since frequency f is known in MRE, wavenumbers are easily converted into shear wave speed SWS, which is a proxy for storage modulus ($SWS = \sqrt{G'/\rho}$). Computing first-order phase gradients is indeed a unique way to avoid second-order noise-sensitive derivatives as required by other solutions of the wave equation [107]. However, the challenge here lies in k_x, the wavenumber in x-direction. Since the acquired field $\widetilde{u}_i(f)$ is a superposition of multidirectional waves, one needs directional filtering to decompose the full field into unidirectional wavenumbers such as k_x and k_y before computing the phase gradient [108]. A similar approach is local frequency estimation (LFE), in which a band of k-space filtered waves is inverted [109]. The lognormal filters used in LFE can be tuned to resemble either first or second derivatives in k-space. Irrespective of whether first or second derivatives are employed, it has been shown that solutions to the inverse problem can be stabilized by multifrequency, multi-component averaging prior to inversion [61,107]. This multi-inversion approach has been termed tomoelastography as it produces viscoelastic parameter maps with a detail resolution similar to that of standard MRI (tomographic) images (see Fig. 4) [65]. In a nutshell, first-order MRE inversion techniques (phase gradient and LFE) fundamentally differ from second-order inversions (direct Helmholtz inversion, variational methods) in that they operate on solutions of the wave equation (plane waves) instead of solving the wave equation itself. Consequently, first-order methods are robust against noise but need preprocessing such as directional filtering, which can degrade detail resolution in SWS maps. In contrast, second-order methods, including Helmholtz inversion, satisfy Huygens' principle of superimposed multisource wave fields and, thus, provide G^*-maps without prior decomposition of wave fields. The parameters that can be retrieved by MRE inversion techniques are summarized in Table 1.

Table 1
Basic tissue parameters that can be measured by MRE. FE: finite element.

Parameter	Symbol (s)	Unit	Explanation	Inversion type
Storage modulus	$\mathrm{Re}(G^*)$, G'	kPa	Real part of complex shear modulus G^*, related to elasticity (colloquially known as stiffness)	Direct inversion, FE inversion
Loss modulus	$\mathrm{Im}(G^*)$, G''	kPa	Imaginary part of G^*, related to viscous loss	Direct inversion, FE inversion
Magnitude modulus	$\lvert G^*\rvert$	kPa	Magnitude of G^*, which mixes elastic and viscous properties, equivalent to stiffness only if $G'' = 0$	Magnitude-based direct inversion
Loss angle / Fluidity	φ	rad	Phase angle of the complex modulus, which is zero in purely elastic materials and $\pi/2$ in viscous fluids	Phase-angle-based direct inversion
Shear wave speed	SWS	m/s	Propagation speed of the induced shear waves (used as a surrogate parameter of stiffness)	Phase gradient
Penetration rate	PR	m/s	Penetration depth of shear waves at $\omega/2\pi$ (used as a surrogate parameter of inverse viscous loss)	Phase gradient
Wavenumber	k	1/m	Local wavenumber at frequency ω	Phase gradient
Wavelength	λ	m	Spatial extension of shear waves (used as a simple ruler for stiffness)	Ruler of stiffness
Damping ratio	γ	–	Ratio of loss to storage properties: $\gamma = G''/(2G')$	Derived from G^*
Young's modulus	E	kPa	Elastic modulus for axial deformation, obtained by $E = 3G^*$ assuming isotropy and incompressibility	Derived from G^*
Kelvin–Voigt model parameters	μ, η	kPa, Pa•s	Elasticity μ and viscosity η based on the Kelvin–Voigt model	Fitting frequency dispersion of G^*
Maxwell model parameters	μ, η	kPa, Pa•s	Elasticity and viscosity based on the Maxwell model	Fitting frequency dispersion of G^*
Spring-pot model parameters	μ, α	kPa, N/A	Elasticity and power law exponent α based on the spring-pot model	Fitting frequency dispersion of G^*

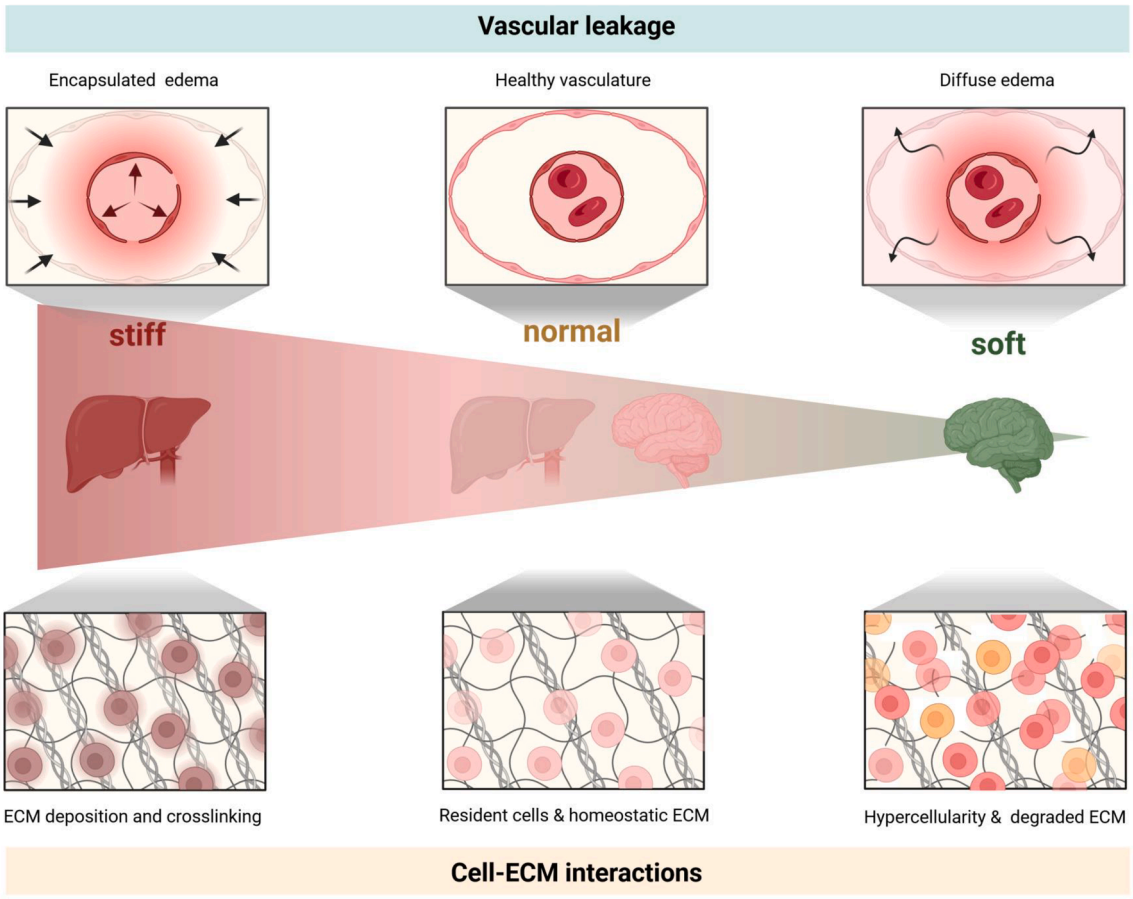

Fig. 5. Fundamental effects of inflammation are associated with stiffness changes in the liver and brain. While hepatic inflammation has been observed to cause tissue stiffening, neuroinflammatory diseases have been associated with softening. Reasons for the different tissue responses are discussed in the text.

4. Applications

In vivo MRE opens the door to a world of biomechanical interactions that are not yet fully understood. According to what we currently know, the convergence of mechanobiology and continuum mechanics is primarily driven by observational studies that address monocausal correlations. Nevertheless, these studies contribute important pieces to the puzzle of which MRE parameters can be used to detect and stage diseases and ultimately predict disease courses. Much insight has been gained from experiments in well-defined phantoms that mimic basic structural features of biological tissues [7,110,111] or modified ex vivo specimens that simulate mechanically relevant processes in vivo [28,112–117]. To provide a hands-on understanding of the basic interactions to which MRE is potentially sensitive, we will not list here the large body of literature on MRE applications but briefly discuss a few studies that highlight the biomechanical effects to be harnessed as diagnostic MRE markers. Moreover, in doing so, we will only discuss pathophysiological hallmarks related to inflammation, from early events in the inflammatory cascade to tissue remodeling at the stage of chronic inflammation. Finally, we attempt to disentangle the mechanical signature of inflammation-affected tissues with a focus on the liver and the brain.

4.1. Vascular leakage, blood perfusion, and pressure

Vascular leakage is a critical initial response of biological tissues to injury and can be seen as a precursor to several subsequent inflammatory and healing processes. The immediate response to tissue injury involves disruption of endothelial glycocalyx and cell junctions at the microvascular level. The resulting increase in vascular permeability fosters the exudation of plasma proteins and fluids into the interstitial space, contributing to the formation of edema. Such edematous accumulation of fluid within soft tissues not only dilutes local toxins and facilitates the entry of immune cells including neutrophils and macrophages but also results in the characteristic swelling of the affected tissue.

While fluid accumulation clearly has a mechanical effect, immune cell migration is unlikely to alter the macroscopic mechanical tissue properties to any degree [118]. Fig. 5 illustrates the different effects of fluid accumulation on the mechanical properties of soft tissues: encapsulated tissues, such as those surrounded by connective tissue and ligaments, cannot expand freely upon fluid infiltration. Therefore, edema is often felt as a firm bump resulting from nonlinear stretching of connective tissue. Similarly, overstretched cell membranes or pressurized blood vessels have been seen as macroscopic stiffening in several MRE studies investigating different scenarios and entities [26]. Fundamental research was performed by Parker et al. who developed a microfluid-flow model and validated it in liver tissue [27,28] and placenta [119]. While a study in sheep livers demonstrated an increase in whole-organ stiffness and elucidated the way in which this was brought about by vascular expansion at higher portal pressure [88], the opposite was observed in smaller specimens such as rat livers [114]. Without the constriction imposed by bulky tissues and promoted by vascular leakage, liver tissue was observed to become softer with increased portal pressure [114]. These two studies nicely illustrate the bidirectional effect of fluids on soft tissue stiffness: confinement promotes stiffening, which is likely related to the generation of tissue pressure, whereas an increase in the fluid content of distensible tissue leads to its expansion and softening [65]. Because the liver capsule prevents expansion, studies in both patients and animal models show correlations between portal pressure and tissue stiffness [120,121]. In healthy volunteers, the

amount of blood perfusing the liver, which can be modulated by breathing [64], abdominal pressure [122,123], eating [124,125], or water intake [65,126], has been found to be an influencing factor affecting liver stiffness. These observations suggest that any change in blood perfusion, including edematous water accumulation, congestion, or increased perfusion pressure, as often associated with inflammation, leads to higher liver stiffness. Since stiffening is also a hallmark of fibrosis, viscosity-related markers such as loss modulus or damping ratio (see Table 1) raise the exciting prospect of distinguishing fluid-driven inflammatory processes from matrix accumulation in fibrosis [120]. Indeed, recent studies in patients have corroborated these findings by demonstrating liver tissue fluidity and damping ratio to be sensitive to inflammation independent of fibrosis [127,128].

In the brain, tissue stiffening generated by vascular effects or driven by fluid accumulation has been observed after formation of cytotoxic edema [129], hypercapnia [130,131], Valsalva maneuver [130], venous drainage [132], functional activation [133,134], elevated intracranial pressure [135,136], and arterial pulsation [137]. All of these stiffening effects may be explained by hyperelastic dilatation of cell membranes or blood vessels, resulting in an overall increase in brain stiffness on a coarse-grained scale. The opposite was reported in scenarios of impaired vascular integrity as a symptom of a disrupted blood–brain barrier [8] or reduced cerebral blood flow due to dehydration [138] or hypothermia [139]. Unlike higher blood perfusion, increased tissue water, as in peritumoral edema, was not associated with marked changes in viscoelasticity, suggesting a fine balance between confinement and expansion of brain tissue [140]. However, in cortical areas, where brain tissue can better expand than in the bulk, the amount of tissue water was negatively associated with stiffness [141]. This observation supports the hypothesis that water content or fluid fraction in the absence of pressure correlates with tissue softening.

Notably, MRE in other organs than the liver and brain revealed similar mechanical patterns upon inflammation, with a tendency toward either liver-like stiffening or brain-like softening. For example, pancreatitis [142,143] and inflammatory bowel disease [144] were associated with markedly elevated tissue stiffness, which, against the soft background of normal pancreatic or colon tissue, provided excellent MRE contrast for detecting local inflammatory activity [145]. Otherwise, nephritis was shown to be associated with significant softening even at asymptomatic filtration rates based on blood markers [146,147]. This soft signature of renal inflammation was likely associated with decreased capillary perfusion pressure and increased free water pools, as discussed above for the brain [148,149].

4.2. Matrix accumulation, crosslinking, and cellular changes

Chronic inflammation of the liver causes matrix accumulation, which is associated with tissue stiffening, making MRE a sensitive biomarker for the noninvasive staging of hepatic fibrosis [59,150–155]. However, collagen deposition in the liver is not a uniform process but exhibits spatial variance and heterogeneous mechanical effects. For example, the outgrowth of collagen fibers from the portal triad into the liver parenchyma establishes a basic network of fiber bundles and can occur without crosslinking [156]. Therefore, the overall effect of septal infiltration on liver stiffness is not necessarily larger than in pericellular fibrosis, where loose collagen aggregates are mainly deposited in the interstitial spaces between hepatocytes [118]. Otherwise, pericellular fibrosis has been associated with increased vascular resistance, which may contribute to the aforementioned cascade of vascular effects on liver stiffness [157]. Beyond the sheer amount of matrix proteins that contribute to the expansion of ECM from 0.3 % in healthy livers to 30 % in cirrhosis, crosslinking and fiber bridging are the critical steps that are expected to increase tissue stiffness by orders of magnitude [47,158]. Therefore, significant stiffening is seen in bridging fibrosis, which is characterized by uninterrupted collagenous septa that form a continuous mechanical mesh over great distances. Although, in histologic slides, bridging fibrosis can be as delicate as septal infiltration or pericellular fibrosis, it represents mechanical gap closures, which usually have larger effects on the stiffness of scaffolds [118]. On the cellular level, inflammation triggers an influx of immune cells into the liver, including macrophages, neutrophils, and lymphocytes, which aim to eliminate pathogens or toxins. In the liver, portal and lobular inflammation are features of Metabolic Dysfunction-associated Steatotic Liver Disease (MASLD), which describes the inflammatory infiltration of the portal triad, primarily by lymphocytes. This cell infiltration is often associated with the formation of edema and, as discussed earlier, may alter the mechanical properties of the tissue, but is unlikely to cause a direct mechanical response related to cell number [118]. Also, in the brain, changes in mechanical properties in cortical areas were not correlated with leukocyte infiltration in experimental autoimmune encephalomyelitis, a mouse model of multiple sclerosis, but rather with chondroitin sulfate remodeling [159]. Because the number of leukocytes in perivascular spaces increases with vascular permeability [160] a significant correlation was found between leukocyte infiltration and brain tissue softening, which, however, is most likely driven by water content rather than cell number [8].

Direct intrinsic cellular responses such as hepatocytic ballooning in MASLD have been observed to increase liver stiffness, probably due to the hyperelastic prestretch of cell membranes and intracellular fluid retention [118]. Moreover, liver stiffness is also affected by metabolic cell function. For example, Shahryari et al. showed that stiff livers in rabbits had a reduced capacity for triacylglycerol storage, but increased gluconeogenesis capacities and increased cholesterol synthesis [161]. In particular, triacylglycerides and cholesterol esters have a role in the production of infectious viruses such as hepatitis C [162]. Antiviral therapy in hepatitis C improves hepatocyte function [163], prompting liver softening as a promising marker for monitoring antiviral therapy [164,165]. It should be noted, though, that aberrant metabolic activity of hepatocytes due to inflammation overlaps with fibrosis, making blood markers such as glutamate–oxaloacetate transaminase for lipotoxicity an important tool for obtaining additional information [166,167]. Also, the hormones released during pregnancy affect the function and activity of the gallbladder and of hepatocytes, leading to reversible stiffening of the liver in pregnant women [168]. Here, bile accumulation, hepatocyte apoptosis, and hypertrophy have been discussed as possible factors causing the observed stiffening of liver tissue [169,170]. Although the specific mechanisms of how cell metabolism relates to tissue mechanics are still vague, we may assume that cellular swelling, prestretched cell membranes, and a shift of water from the extracellular pool into cells partially contribute to the sensitivity of MRE to liver function [169]. How drastically the macroscopic biomechanical properties of the liver change upon disruption of cell membranes can be seen after freezing and thawing liver tissue. MRE and histology showed that cell membrane disruption and sinusoidal endothelial cell detachment reduce tissue stiffness by a factor of 10 [116]. Similar mechanisms occur in the brain, where neuronal swelling and cytotoxic edema formation in the course of dying were found to lead to a marked increase in tissue stiffness [129].

Conversely, processes involved in neuroinflammation underlying multiple sclerosis (MS) or neuromyelitis optica have been shown to be associated with brain softening [171–174]. In experimental autoimmune encephalomyelitis (EAE), the animal model of MS, MRE detected softening in areas where contrast-enhanced MRI showed typical hallmarks of neuroinflammation, such as gliosis, leukocyte extravasation, and reduced sulfation of glycosaminoglycans [8]. Similarly, the extent of tissue remodeling at sites of blood–brain barrier disruption, as indicated by fibronectin overexpression in acute EAE lesions, correlated with the degree of tissue softening in the mouse cerebellum [175,176]. In EAE, fibronectin reflects the detachment of astrocytic endfeet from blood vessels with weakening of glial-vascular mechanical cross-links and thus tissue softening. This mechanism partially explains why the brain softens during the acute phase of EAE and stiffens during EAE remission [176,177]. In addition, adhesion of neurons to their matrix

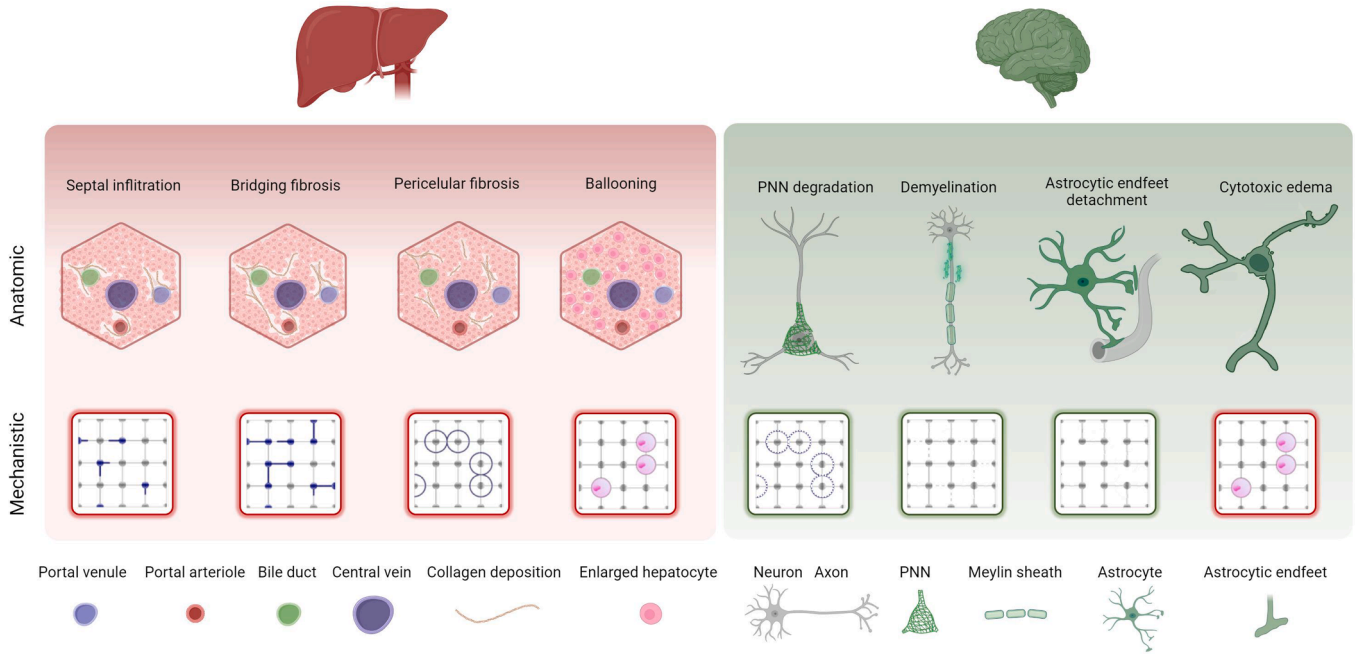

Fig. 6. Biomechanical effects of abnormal events related to inflammatory processes in the liver and the brain. As discussed, MRE has been proven sensitive to all of these changes in tissue structure.

through perineuronal networks (PNN) plays a critical role in brain stiffness. Therefore, PNN degradation has been shown to be associated with tissue softening following the remitting-relapsing course of EAE [159]. This loss of PNN integrity in cortical brain regions is specific to inflammation and is associated with marked tissue softening, which is why MRE has been proposed as an imaging marker of cortical tissue involvement in MS patients [159]. Neuroinflammation is a good example of the emergent effects of different substructures on coarse-grained mechanical tissue properties. Mechanical weakening of dendrites through demyelination [178], detachment of astrocytic endfeet from microvessels [176], and PNN degradation [159] – these processes collectively shape the mechanical response of the brain to neuroinflammation and prompt tissue softening as an MRE marker for treatment monitoring in MS.

Fig. 6 summarizes viscoelastic matrix remodeling and cellular changes reported in association with hepatic and neuronal inflammation.

Overall, the reports discussed here illustrate the sensitivity of MRE to tissue remodeling and inflammation-related processes. Soft tissues affected by inflammation develop their own specific signatures of changes in mechanical properties, which are potentially detectable by MRE. Detection and staging of inflammation could provide early warning of many diseases and thus allow initiation of individualized therapies before the development of serious symptoms, end-stage diseases, such as cancer, or whole-organ failure. However, it remains to be seen how MRE can be further sensitized to the discussed mechanical features of inflammation – from vascular leakage to cell swelling, to matrix changes. For example, MRE could be tailored towards higher sensitivities to fluid–solid interactions by the use of low-frequency vibrations [25,179] or shear wave dispersion quantification as a measure of tissue fluidity [180].

5. Brief summary

MRE is a versatile technique for imaging the biomechanical properties of soft tissues across a wide range of resolutions, mechanical frequencies, and applications in both clinical diagnosis and biomedical research. By encoding time-harmonic mechanical vibrations using phase-contrast MRI techniques, MRE is an imaging modality that works by capturing shear waves propagating through body tissues. MRE relies on the inversion of shear wave images into viscoelastic parameter maps. The setup of an MRE experiment on clinical MRI scanners is now a standardized procedure that adds diagnostic value to the detection and staging of diseases along the entire pathological cascade of inflammation-associated tissue remodeling from early edema to chronic fibrosis, cirrhosis, and cancer. Despite the overwhelming evidence for MRE sensitivity to inflammation, further research is needed to disentangle the biomechanical hallmarks of inflammation discussed in this article: vascular leakage, altered blood flow, elevated tissue pressure, increased fluid fraction, cellular edema, matrix accumulation, and remodeling.

CRediT authorship contribution statement

Tom Meyer: Conceptualization, Methodology, Writing – review & editing. **Johannes Castelein:** Visualization, Writing – review & editing. **Jakob Schattenfroh:** Visualization, Writing – review & editing. **Anna Sophie Morr:** Visualization, Writing – review & editing. **Rafaela Vieira da Silva:** Visualization, Writing – review & editing. **Heiko Tzschätzsch:** Methodology, Writing – original draft. **Rolf Reiter:** Validation, Writing – original draft. **Jing Guo:** Methodology, Validation, Writing – original draft. **Ingolf Sack:** Writing – original draft, Visualization, Methodology, Investigation, Funding acquisition, Formal analysis, Conceptualization.

Declaration of competing interest

The authors declare that they have no known competing financial interests or personal relationships that could have appeared to influence the work reported in this paper.

Data availability

No data was used for the research described in the article.

Acknowledgements

German Research Foundation (FOR5628, 460333672 CRC1540 EBM, CRC1340, GRK2260 BIOQIC)

References

[1] P.C. Georges, J.J. Hui, Z. Gombos, M.E. McCormick, A.Y. Wang, M. Uemura, R. Mick, P.A. Janmey, E.E. Furth, R.G. Wells, Increased stiffness of the rat liver precedes matrix deposition: implications for fibrosis, Am J Physiol Gastrointest Liver Physiol 293 (6) (2007) G1147–G1154.
[2] W. Fan, K. Adebowale, L. Vancza, Y. Li, M.F. Rabbi, K. Kunimoto, D. Chen, G. Mozes, D.K. Chiu, Y. Li, J. Tao, Y. Wei, N. Adeniji, R.L. Brunsing, R. Dhanasekaran, A. Singhi, D. Geller, S.H. Lo, L. Hodgson, E.G. Engleman, G. W. Charville, V. Charu, S.P. Monga, T. Kim, R.G. Wells, O. Chaudhuri, N.J. Torok, Matrix viscoelasticity promotes liver cancer progression in the pre-cirrhotic liver, Nature 626 (7999) (2024) 635–642.
[3] S. Mueller, Does pressure cause liver cirrhosis? The sinusoidal pressure hypothesis, World J Gastroenterol 22 (48) (2016) 10482–10501.
[4] C.E. Keating, D.K. Cullen, Mechanosensation in traumatic brain injury, Neurobiol Dis 148 (2021) 105210.
[5] H. Nakagami, Mechanisms underlying the bidirectional association between nonalcoholic fatty liver disease and hypertension, Hypertension Research 46 (2) (2023) 539–541.
[6] V. Mittelheisser, V. Gensbittel, L. Bonati, W. Li, L. Tang, J.G. Goetz, Evidence and therapeutic implications of biomechanically regulated immunosurveillance in cancer and other diseases, Nat Nanotechnol 19 (3) (2024) 281–297.
[7] K.J. Parker, J. Ormachea, M.G. Drage, H. Kim, Z. Hah, The biomechanics of simple steatosis and steatohepatitis, Physics in Medicine & Biology 63 (10) (2018).
[8] R.V. Silva, A.S. Morr, S. Mueller, S.P. Koch, P. Boehm-Sturm, Y. Rodriguez-Sillke, D. Kunkel, H. Tzschatzsch, A.A. Kuhl, J. Schnorr, M. Taupitz, I. Sack, C. Infante-Duarte, Contribution of Tissue Inflammation and Blood-Brain Barrier Disruption to Brain Softening in a Mouse Model of Multiple Sclerosis, Front Neurosci 15 (2021) 701308.
[9] I. Sack, K. Joehrens, E. Wuerfel, J. Braun, Structure sensitive elastography: on the viscoelastic powerlaw behavior of in vivo human tissue in health and disease, Soft Matter 9 (24) (2013) 5672–5680.
[10] I. Sack, Magnetic resonance elastography from fundamental soft-tissue mechanics to diagnostic imaging, Nature Reviews Physics 5 (2023) 25–42.
[11] F. Sauer, S. Grosser, M. Shahryari, A. Hayn, J. Guo, J. Braun, S. Briest, B. Wolf, B. Aktas, L.C. Horn, I. Sack, J.A. Kas, Changes in Tissue Fluidity Predict Tumor Aggressiveness In Vivo, Adv Sci (weinh) 10 (26) (2023) e2303523.
[12] S. Hirsch, J. Braun, I. Sack, Magnetic Resonance Elastography: Physical Background And Medical, Wiley-VCH, Applications, 2017.
[13] J. Ormachea, K.J. Parker, Elastography imaging: the 30 year perspective, Physics in Medicine and Biology 65 (24) (2020).
[14] H. Tzschätzsch, Methods and Approaches in Ultrasound Elastography, in: I. Sack, T. Schaeffter (Eds.), Quantification of Biophysical Parameters in Medical Imaging, Springer, 2017.
[15] R. Muthupillai, D.J. Lomas, P.J. Rossman, J.F. Greenleaf, A. Manduca, R. L. Ehman, Magnetic resonance elastography by direct visualization of propagating acoustic strain waves, Science 269 (5232) (1995) 1854–1857.
[16] A. Ozturk, M.C. Olson, A.E. Samir, S.K. Venkatesh, Liver fibrosis assessment: MR and US elastography, Abdom Radiol (NY) 47 (9) (2022) 3037–3050.
[17] J. Oudry, J. Chen, K.J. Glaser, V. Miette, L. Sandrin, R.L. Ehman, Cross-validation of magnetic resonance elastography and ultrasound-based transient elastography: a preliminary phantom study, J Magn Reson Imaging 30 (5) (2009) 1145–1150.
[18] A.S. Morr, H. Herthum, F. Schrank, S. Görner, M.S. Anders, M. Lerchbaumer, H. P. Müller, T. Fischer, K.V. Jenderka, H.H.G. Hansen, P.A. Janmey, J. Braun, I. Sack, H. Tzschätzsch, Liquid-Liver Phantom: Mimicking the Viscoelastic Dispersion of Human Liver for Ultrasound- and MRI-Based Elastography, Invest Radiol 57 (8) (2022) 502–509.
[19] S.F. Bensamoun, L. Wang, L. Robert, F. Charleux, J.P. Latrive, H.B. Tho, Mc., Measurement of liver stiffness with two imaging techniques: magnetic resonance elastography and ultrasound elastometry, JMagnResonImag 28 (5) (2008) 1287–1292.
[20] H. Tzschatzsch, S. Ipek-Ugay, M. Nguyen Trong, J. Guo, J. Eggers, E. Gentz, T. Fischer, M. Schultz, J. Braun, I. Sack, Multifrequency Time-Harmonic Elastography for the Measurement of Liver Viscoelasticity in Large Tissue Windows, Ultrasound Med Biol 41 (3) (2015) 724–733.
[21] Klemmer Chandía S, Schattenfroh J, Brinker S, Tzschätzsch H, Meyer T, Sack I. Cross-validating magnetic resonance elastography and ultrasound time-harmonic elastography of the brain by using a 3D optical tracker. In: Proc 32nd Annual Meeting ISMRM; 2024; Singapore. p PP-21.
[22] A. Manduca, P.J. Bayly, R.L. Ehman, A. Kolipaka, T.J. Royston, I. Sack, R. Sinkus, B.E. Van Beers, MR elastography: Principles, guidelines, and terminology, Magn Reson Med 85 (5) (2021) 2377–2390.
[23] S. Hirsch, A Biphasic Poroelastic Model for Soft Tissues, in: I. Sack, T. Schaeffter (Eds.), Quantification of Biophysical Parameters in Medical Imaging, 1st ed., Springer, Heidelberg, 2018, p. 71.
[24] A.P. Sarvazyan, A.R. Skovoroda, S.Y. Emelianov, J.B. Fowlkes, J.G. Pipe, R.S. Adler, R.B. Buxton, P.L. Carson, editors. Biophysical Bases of Elasticity Imaging. Volume 21. New York: Plenum Press; 1995. 223-240 p.
[25] M.D. McGarry, C.L. Johnson, B.P. Sutton, J.G. Georgiadis, E.E. Van Houten, A. J. Pattison, J.B. Weaver, K.D. Paulsen, Suitability of poroelastic and viscoelastic mechanical models for high and low frequency MR elastography, Med Phys 42 (2) (2015) 947.
[26] J. Guo, F. Schwahofer, J. Braun, Sensitivity of tissue shear stiffness to pressure and perfusion in health and disease, in: I. Sack, T. Schaeffter (Eds.), Quantification of Biophysical Parameters in Medical Imaging, 2 ed:, Springer, 2024.
[27] K.J. Parker, A microchannel flow model for soft tissue elasticity, Phys Med Biol 59 (15) (2014) 4443–4457.
[28] K.J. Parker, Experimental evaluations of the microchannel flow model, Phys Med Biol 60 (11) (2015) 4227–4242.
[29] S. Hirsch, T. Schaeffter, I. Sack, The fundamentals of transport in living tissues quantified by medical imaging technologies, in: I. Sack, T. Schaeffter (Eds.), Quantification of Biophysical Parameters in Medical Imaging, 2nd ed., Springer, Heidelberg, 2024, p. 9.
[30] K.J. Streitberger, L. Lilaj, F. Schrank, J. Braun, K.T. Hoffmann, M. Reiss-Zimmermann, J.A. Käs, I. Sack, How tissue fluidity influences brain tumor progression, Proc Natl Acad Sci U S A 117 (1) (2020) 128–134.
[31] D. Klatt, U. Hamhaber, P. Asbach, J. Braun, I. Sack, Noninvasive assessment of the rheological behavior of human organs using multifrequency MR elastography: A study of brain and liver viscoelasticity, Phys Med Biol 52 (24) (2007) 7281–7294.
[32] S.S. Poul, J. Ormachea, G.R. Ge, K.J. Parker, Comprehensive experimental assessments of rheological models' performance in elastography of soft tissues, Acta Biomater (2022).
[33] A.P. Sarvazyan, M.W. Urban, J.F. Greenleaf, Acoustic waves in medical imaging and diagnostics, Ultrasound Med Biol 39 (7) (2013) 1133–1146.
[34] M.D.J. McGarry, E.E.W. Van Houten, P.R. Perrinez, A.J. Pattison, J.B. Weaver, K. D. Paulsen, An octahedral shear strain-based measure of SNR for 3D MR elastography, Physics in Medicine and Biology 56 (13) (2011) N153–N164.
[35] J. Rump, D. Klatt, J. Braun, C. Warmuth, I. Sack, Fractional encoding of harmonic motions in MR elastography, Magn Reson Med 57 (2) (2007) 388–395.
[36] L.V. Hiscox, C.L. Johnson, E. Barnhill, M.D. McGarry, J. Huston, E.J. van Beek, J. M. Starr, N. Roberts, Magnetic resonance elastography (MRE) of the human brain: technique, findings and clinical applications, Phys Med Biol 61 (24) (2016) R401–R437.
[37] I.S. Idilman, J. Li, M. Yin, S.K. Venkatesh, MR elastography of liver: current status and future perspectives, Abdom Radiol (NY) 45 (11) (2020) 3444–3462.
[38] A. Arani, K.L. Glaser, S.P. Arunachalam, P.J. Rossman, D.S. Lake, J.D. Trzasko, A. Manduca, K.P. McGee, R.L. Ehman, P.A. Araoz, In vivo, high-frequency three-dimensional cardiac MR elastography: Feasibility in normal volunteers, Magnetic Resonance in Medicine 77 (1) (2017) 351–360.
[39] P. Asbach, S.R. Ro, N. Aldoj, J. Snellings, R. Reiter, J. Lenk, T. Kohlitz, M. Haas, J. Guo, B. Hamm, J. Braun, I. Sack, In Vivo Quantification of Water Diffusion, Stiffness, and Tissue Fluidity in Benign Prostatic Hyperplasia and Prostate Cancer, Invest Radiol 55 (8) (2020) 524–530.
[40] Y. Deng, Z. Yi, T. Zhang, B. Hu, L. Zhang, K. Rajlawot, S. Kuang, B. He, A. Arani, J. Chen, M. Yin, P. Rossman, K.J. Glaser, S.K. Venkatesh, R.L. Ehman, J. Wang, Magnetic resonance elastography of the prostate in patients with lower urinary tract symptoms: feasibility of the modified driver at high multi-frequencies, Abdom Radiol (NY) 47 (1) (2022) 399–408.
[41] F. Dittmann, S. Hirsch, H. Tzschatzsch, J. Guo, J. Braun, I. Sack, In Vivo Wideband Multifrequency MR Elastography of the Human Brain and Liver, Magnetic Resonance in Medicine 76 (4) (2016) 1116–1126.
[42] H. Herthum, S.C.H. Dempsey, A. Samani, F. Schrank, M. Shahryari, C. Warmuth, H. Tzschatzsch, J. Braun, I. Sack, Supervicous properties of the in vivo brain at large scales, Acta Biomater 121 (2021) 393–404.
[43] T.K. Yasar, T.J. Royston, R.L. Magin, Wideband MR elastography for viscoelasticity model identification, Magn Reson Med 70 (2) (2013) 479–489.
[44] Y.F. Liu, T.K. Yasar, T.J. Royston, Ultra wideband (0.5-16 kHz) MR elastography for robust shear viscoelasticity model identification, Physics in Medicine and Biology 59 (24) (2014) 7717–7734.
[45] R. Reiter, C. Freise, K. Jöhrens, C. Kamphues, D. Seehofer, M. Stockmann, R. Somasundaram, P. Asbach, J. Braun, A. Samani, I. Sack, Wideband MRE and static mechanical indentation of human liver specimen: Sensitivity of viscoelastic constants to the alteration of tissue structure in hepatic fibrosis, J Biomech 47 (7) (2014) 1665–1674.
[46] E.H. Clayton, J.R. Garbow, P.V. Bayly, Frequency-dependent viscoelastic parameters of mouse brain tissue estimated by MR elastography, Phys Med Biol 56 (8) (2011) 2391–2406.
[47] J. Braun, H. Tzschatzsch, C. Korting, A. Ariza de Schellenberger, M. Jenderka, T. Driessle, M. Ledwig, I. Sack, A compact 0.5 T MR elastography device and its application for studying viscoelasticity changes in biological tissues during progressive formalin fixation, Magn Reson Med 79 (1) (2018) 470–478.
[48] P.V. Bayly, J.R. Garbow, Pre-clinical MR elastography: Principles, techniques, and applications, J Magn Reson 291 (2018) 73–83.
[49] G. Bertalan, J. Becker, H. Tzschatzsch, A. Morr, H. Herthum, M. Shahryari, R. D. Greenhalgh, J. Guo, L. Schroder, C. Alzheimer, S. Budday, K. Franze, J. Braun, I. Sack, Mechanical behavior of the hippocampus and corpus callosum: An attempt to reconcile ex vivo with in vivo and micro with macro properties, J Mech Behav Biomed Mater 138 (2023) 105613.
[50] F. Sauer, A. Fritsch, S. Grosser, S. Pawlizak, T. Kiessling, M. Reiss-Zimmermann, M. Shahryari, W.C. Muller, K.T. Hoffmann, J.A. Kas, I. Sack, Whole tissue and single cell mechanics are correlated in human brain tumors, Soft Matter (2021).
[51] A.S. Morr, M. Nowicki, G. Bertalan, R. Vieira Silva, C. Infante Duarte, S.P. Koch, P. Boehm-Sturm, U. Krugel, J. Braun, B. Steiner, J.A. Kas, T. Fuhs, I. Sack,

Mechanical properties of murine hippocampal subregions investigated by atomic force microscopy and in vivo magnetic resonance elastography, Sci Rep 12 (1) (2022) 16723.
[52] D. Gallichan, M.D. Robson, A. Bartsch, K.L. Miller, TREMR: Table-resonance elastography with MR, Magn Reson Med 62 (3) (2009) 815–821.
[53] Uffman K, Grote W, Abicht C, Quick HH, Ladd ME. A piezoelectric actuator for MR elastography. In: Proc 10th Intl Soc Magn Reson Med; 2002; Honolulu. p 2595.
[54] S. Hirsch, J. Guo, R. Reiter, S. Papazoglou, T. Kroencke, J. Braun, I. Sack, MR Elastography of the Liver and the Spleen Using a Piezoelectric Driver, Single-Shot Wave-Field Acquisition, and Multifrequency Dual Parameter Reconstruction, Magn Reson Med 71 (1) (2014) 267–277.
[55] J. Braun, K. Braun, I. Sack, Electromagnetic actuator for generating variably oriented shear waves in MR elastography, Magn Reson Med 50 (1) (2003) 220–222.
[56] R.S. Sahebjavaher, S. Frew, A. Bylinskii, L. ter Beek, P. Garteiser, M. Honarvar, R. Sinkus, S. Salcudean, Prostate MR elastography with transperineal electromagnetic actuation and a fast fractionally encoded steady-state gradient echo sequence, NMR Biomed 27 (7) (2014) 784–794.
[57] Y. Feng, M. Zhu, S. Qiu, P. Shen, S. Ma, X. Zhao, C.H. Hu, L. Guo, A multi-purpose electromagnetic actuator for magnetic resonance elastography, Magn Reson Imaging 51 (2018) 29–34.
[58] Klatt D, Asbach P, Rump J, Papazoglou S, Hamhaber U, Braun J, Sack I. Fast planar steady-state free precession MR elastography on human liver. In: Proc 14th Annual Meeting ISMRM; 2006; Seattle. p 399.
[59] M. Yin, J.A. Talwalkar, K.J. Glaser, A. Manduca, R.C. Grimm, P.J. Rossman, J. L. Fidler, R.L. Ehman, Assessment of hepatic fibrosis with magnetic resonance elastography, Clin Gastroenterol Hepatol 5 (10) (2007) 1207–1213 e1202.
[60] J.H. Runge, S.H. Hoelzl, J. Sudakova, A.S. Dokumaci, J.L. Nelissen, C. Guenthner, J. Lee, M. Troelstra, D. Fovargue, J. Stoker, A.J. Nederveen, D. Nordsletten, R. Sinkus, A novel magnetic resonance elastography transducer concept based on a rotational eccentric mass: preliminary experiences with the gravitational transducer, Physics in Medicine and Biology 64 (4) (2019).
[61] F. Dittmann, R. Reiter, J. Guo, M. Haas, P. Asbach, T. Fischer, J. Braun, I. Sack, Tomoelastography of the prostate using multifrequency MR elastography and externally placed pressurized-air drivers, Magn Reson Med 79 (3) (2018) 1325–1333.
[62] K. Uffmann, M.E. Ladd, Actuation systems for MR elastography: design and applications, IEEE Eng Med Biol Mag 27 (3) (2008) 28–34.
[63] E.R. Triolo, O. Khegai, E. Ozkaya, N. Rossi, A. Alipour, L. Fleysher, P. Balchandani, M. Kurt, Design, Construction, and Implementation of a Magnetic Resonance Elastography Actuator for Research Purposes, Curr Protoc 2 (3) (2022) e379.
[64] M. Anders, T. Meyer, C. Warmuth, J. Pfeuffer, H. Tzschaetzsch, H. Herthum, M. Shahryari, K. Degenhardt, O. Wieben, S. Schmitter, J. Schulz-Menger, T. Schaeffter, J. Braun, I. Sack, Rapid MR elastography of the liver for subsecond stiffness sampling, Magn Reson Med 91 (1) (2024) 312–324.
[65] F. Dittmann, H. Tzschatzsch, S. Hirsch, E. Barnhill, J. Braun, I. Sack, J. Guo, Tomoelastography of the abdomen: Tissue mechanical properties of the liver, spleen, kidney, and pancreas from single MR elastography scans at different hydration states, Magn Reson Med 78 (3) (2017) 976–983.
[66] M.A. Bernstein, K.F. King, X.J. Zhou, Handbook of MRI pulse sequences, Elsevier Academic Press, Burlington, 2004.
[67] R. Sinkus, J. Lorenzen, D. Schrader, M. Lorenzen, M. Dargatz, D. Holz, High-resolution tensor MR elastography for breast tumour detection, Phys Med Biol 45 (6) (2000) 1649–1664.
[68] M. Shahryari, T. Meyer, C. Warmuth, H. Herthum, G. Bertalan, H. Tzschatzsch, L. Stencel, S. Lukas, L. Lilaj, J. Braun, I. Sack, Reduction of breathing artifacts in multifrequency magnetic resonance elastography of the abdomen, Magn Reson Med 85 (4) (2021) 1962–1973.
[69] E. Barnhill, M. Nikolova, C. Ariyurek, F. Dittmann, J. Braun, I. Sack, Fast Robust Dejitter and Interslice Discontinuity Removal in MRI Phase Acquisitions: Application to Magnetic Resonance Elastography, IEEE Trans Med Imaging 38 (7) (2019) 1578–1587.
[70] T.J. Flynn, Two-dimensional phase unwrapping with minimum weighted discontinuity, Journal of the Optical Society of America a-Optics Image Science and Vision 14 (10) (1997) 2692–2701.
[71] Z. Yin, Y. Sui, J.D. Trzasko, P.J. Rossman, A. Manduca, R.L. Ehman, J. Huston, In vivo characterization of 3D skull and brain motion during dynamic head vibration using magnetic resonance elastography, Magnetic Resonance in Medicine 80 (6) (2018) 2573–2585.
[72] H. Herthum, H. Carrillo, A. Osses, S. Uribe, I. Sack, C. Bertoglio, Multiple motion encoding in phase-contrast MRI: A general theory and application to elastography imaging, Med Image Anal 78 (2022) 102416.
[73] Barnhill E, Kennedy P, Johnson CL, Mada M, Roberts N. Real-time 4D phase unwrapping applied to magnetic resonance elastography. Magn Reson Med 2014: [Epub ahead of print] doi: 10.1002/mrm.25332.
[74] S. Papazoglou, S. Hirsch, J. Braun, I. Sack, Multifrequency inversion in magnetic resonance elastography, Phys Med Biol 57 (8) (2012) 2329–2346.
[75] D. Fovargue, D. Nordsletten, R. Sinkus, Stiffness reconstruction methods for MR elastography, NMR Biomed 31 (10) (2018) e3935.
[76] M.M. Doyley, Model-based elastography: a survey of approaches to the inverse elasticity problem, Phys Med Biol 57 (3) (2012) R35–R73.
[77] I. Sack, C.K. McGowan, A. Samani, C. Luginbuhl, W. Oakden, D.B. Plewes, Observation of nonlinear shear wave propagation using magnetic resonance elastography, Magn Reson Med 52 (4) (2004) 842.
[78] M. McGarry, E. Van Houten, D. Sowinski, D. Jyoti, D.R. Smith, D.A. Caban-Rivera, G. McIlvain, P. Bayly, C.L. Johnson, J. Weaver, K. Paulsen, Mapping heterogenous anisotropic tissue mechanical properties with transverse isotropic nonlinear inversion MR elastography, Med Image Anal 78 (2022) 102432.
[79] Y. Feng, R.J. Okamoto, R. Namani, G.M. Genin, P.V. Bayly, Measurements of mechanical anisotropy in brain tissue and implications for transversely isotropic material models of white matter, J Mech Behav Biomed Mater 23C (2013) 117–132.
[80] S. Papazoglou, J. Rump, J. Braun, I. Sack, Shear-wave group-velocity inversion in MR elastography of human skeletal muscle, Magn Reson Med 56 (3) (2006) 489–497.
[81] J. Guo, S. Hirsch, M. Scheel, J. Braun, I. Sack, Three-Parameter Shear Wave Inversion in MR Elastography of Incompressible Transverse Isotropic Media: Application to In Vivo Lower Leg Muscles, Magnetic Resonance in Medicine 75 (4) (2016) 1537–1545.
[82] B. Babaei, D. Fovargue, R.A. Lloyd, R. Miller, L. Juge, M. Kaplan, R. Sinkus, D. A. Nordsletten, L.E. Bilston, Magnetic Resonance Elastography Reconstruction for Anisotropic Tissues, Med Image Anal 74 (2021) 102212.
[83] P.E. Barbone, A.A. Oberai, Elastic modulus imaging: some exact solutions of the compressible elastography inverse problem, Physics in Medicine and Biology 52 (6) (2007) 1577–1593.
[84] J.R. McLaughlin, N. Zhang, A. Manduca, Calculating tissue shear modulus and pressure by 2D Log-Elastographic methods, Inverse Probl 26 (8) (2010).
[85] A.J. Romano, J.J. Shirron, J.A. Bucaro, On the noninvasive determination of material parameters from a knowledge of elastic displacements theory and numerical simulation, IEEE Trans Ultrason Ferroelectr Freq Control 45 (3) (1998) 751–759.
[86] P.J. Davies, I. Sack, A stacked frequency approach for inhomogeneous time-dependent MRE: an inverse problem for the elastic shear modulus, Ima Journal of Applied Mathematics 86 (1) (2021) 121–145.
[87] P.J. Davies, E. Barnhill, I. Sack, THE MRE INVERSE PROBLEM FOR THE ELASTIC SHEAR MODULUS, Siam Journal on Applied Mathematics 79 (4) (2019) 1367–1388.
[88] S. Hirsch, J. Guo, R. Reiter, E. Schott, C. Buning, R. Somasundaram, J. Braun, I. Sack, T.J. Kroencke, Towards compression-sensitive magnetic resonance elastography of the liver: Sensitivity of harmonic volumetric strain to portal hypertension, J Magn Reson Imaging 39 (2) (2014) 298–306.
[89] S. Hirsch, D. Klatt, F. Freimann, M. Scheel, J. Braun, I. Sack, In vivo measurement of volumetric strain in the human brain induced by arterial pulsation and harmonic waves, Magn Reson Med 70 (3) (2012) 671–683.
[90] G. Page, M. Tardieu, L. Besret, L. Blot, J. Lopes, R. Sinkus, B.E. Van Beers, P. Garteiser, Assessing Tumor Mechanics by MR Elastography at Different Strain Levels, J Magn Reson Imaging 50 (6) (2019) 1982–1989.
[91] G. Page, M. Tardieu, J.L. Gennisson, L. Besret, P. Garteiser, B.E. Van Beers, Tumor Solid Stress: Assessment with MR Elastography under Compression of Patient-Derived Hepatocellular Carcinomas and Cholangiocarcinomas Xenografted in Mice, Cancers (basel) 13 (8) (2021).
[92] D. Fovargue, M. Fiorito, A. Capilnasiu, D. Nordsletten, J. Lee, R. Sinkus, Towards noninvasive estimation of tumour pressure by utilising MR elastography and nonlinear biomechanical models: a simulation and phantom study, Scientific Reports 10 (1) (2020).
[93] T. Elgeti, J. Rump, S. Papazoglou, U. Hamhaber, B. Hamm, J. Braun, I. Sack, Cardiac magnetic resonance elastography – initial results, Invest Radiol 43 (11) (2008) 762–772.
[94] F. Fakhouri, M. Joseph, M. Ballinger, V. Shukla, D. Weimar, C. Novak, S. Ghadiali, A. Kolipaka, Magnetic Resonance Elastography (MRE) of Bleomycin-Induced Pulmonary Fibrosis in an Animal Model, Invest Radiol 58 (4) (2023) 299–306.
[95] A. Kolipaka, P.A. Araoz, K.P. McGee, A. Manduca, R.L. Ehman, Magnetic resonance elastography as a method for the assessment of effective myocardial stiffness throughout the cardiac cycle, Magn Reson Med 64 (3) (2010) 862–870.
[96] J. Mura, F. Schrank, I. Sack, An analytical solution to the dispersion-by-inversion problem in magnetic resonance elastography, Magn Reson Med 84 (1) (2020) 61–71.
[97] S. Papazoglou, U. Hamhaber, J. Braun, I. Sack, Algebraic Helmholtz inversion in planar magnetic resonance elastography, Phys Med Biol 53 (12) (2008) 3147–3158.
[98] K.P. McGee, D. Lake, Y. Mariappan, R.D. Hubmayr, A. Manduca, K. Ansell, R. L. Ehman, Calculation of shear stiffness in noise dominated magnetic resonance elastography data based on principal frequency estimation, Phys Med Biol 56 (14) (2011) 4291–4309.
[99] R.S. Anderssen, M. Hegland, For numerical differentiation, dimensionality can be a blessing!, Math Comput 68 (227) (1999) 1121–1141.
[100] E. Barnhill, L. Hollis, I. Sack, J. Braun, P.R. Hoskins, P. Pankaj, C. Brown, E.J. R. van Beek, N. Roberts, Nonlinear multiscale regularisation in MR elastography: Towards fine feature mapping, Med Image Anal 35 (2017) 133–145.
[101] M.D. McGarry, E.E. Van Houten, C.L. Johnson, J.G. Georgiadis, B.P. Sutton, J. B. Weaver, K.D. Paulsen, Multiresolution MR elastography using nonlinear inversion, Med Phys 39 (10) (2012) 6388–6396.
[102] E.E. Van Houten, K.D. Paulsen, M.I. Miga, F.E. Kennedy, J.B. Weaver, An overlapping subzone technique for MR-based elastic property reconstruction, Magn Reson Med 42 (4) (1999) 779–786.
[103] A. Baghani, S. Salcudean, M. Honarvar, R.S. Sahebjavaher, R. Rohling, R. Sinkus, Travelling wave expansion: a model fitting approach to the inverse problem of elasticity reconstruction, IEEE Trans Med Imaging 30 (8) (2011) 1555–1565.
[104] J.M. Scott, A. Arani, A. Manduca, K.P. McGee, J.D. Trzasko, J. Huston 3rd, R. L. Ehman, M.C. Murphy, Artificial neural networks for magnetic resonance

elastography stiffness estimation in inhomogeneous materials, Med Image Anal 63 (2020) 101710.
[105] S. Ma, R. Wang, S. Qiu, R. Li, Q. Yue, Q. Sun, L. Chen, F. Yan, G.Z. Yang, Y. Feng, MR Elastography With Optimization-Based Phase Unwrapping and Traveling Wave Expansion-Based Neural Network (TWENN), IEEE Trans Med Imaging 42 (9) (2023) 2631–2642.
[106] A. Manduca, T.E. Oliphant, M.A. Dresner, J.L. Mahowald, S.A. Kruse, E. Amromin, J.P. Felmlee, J.F. Greenleaf, R.L. Ehman, Magnetic resonance elastography: non-invasive mapping of tissue elasticity, Med Image Anal 5 (4) (2001) 237–254.
[107] H. Tzschatzsch, J. Guo, F. Dittmann, S. Hirsch, E. Barnhill, K. Johrens, J. Braun, I. Sack, Tomoelastography by multifrequency wave number recovery from time-harmonic propagating shear waves, Medical Image Analysis 30 (2016) 1–10.
[108] A. Manduca, D.S. Lake, S.A. Kruse, R.L. Ehman, Spatio-temporal directional filtering for improved inversion of MR elastography images, Med Image Anal 7 (4) (2003) 465–473.
[109] H. Knutsson, C.J. Westin, G. Granlund, Local multiscale frequency and bandwidth estimation, in: In: Proc of the IEEE Intl Conf on Image Processing, 1994, pp. 36–40.
[110] J. Guo, O. Posnansky, S. Hirsch, M. Scheel, M. Taupitz, J. Braun, I. Sack, Fractal network dimension and viscoelastic powerlaw behavior: II. An experimental study of structure-mimicking phantoms by magnetic resonance elastography, Phys Med Biol 57 (12) (2012) 4041–4053.
[111] S.A. Lambert, S.P. Nasholm, D. Nordsletten, C. Michler, L. Juge, J.M. Serfaty, L. Bilston, B. Guzina, S. Holm, R. Sinkus, Bridging Three Orders of Magnitude: Multiple Scattered Waves Sense Fractal Microscopic Structures via Dispersion, Phys Rev Lett 115 (9) (2015) 094301.
[112] M. Perepelyuk, L. Chin, X. Cao, A. van Oosten, V.B. Shenoy, P.A. Janmey, R. G. Wells, Normal and Fibrotic Rat Livers Demonstrate Shear Strain Softening and Compression Stiffening: A Model for Soft Tissue Mechanics, PLoS One 11 (1) (2017) e0146588.
[113] M.D. Nieskoski, K. Marra, J.R. Gunn, S.C. Kanick, M.M. Doyley, T. Hasan, S. P. Pereira, B.S. Trembly, B.W. Pogue, Separation of Solid Stress From Interstitial Fluid Pressure in Pancreas Cancer Correlates With Collagen Area Fraction, Journal of Biomechanical Engineering-Transactions of the Asme 139 (6) (2017).
[114] Y. Safraou, K. Krehl, T. Meyer, S. Mehrgan, J.E.L. Jordan, H. Tzschatzsch, T. Fischer, P. Asbach, J. Braun, I. Sack, J. Guo, The influence of static portal pressure on liver biophysical properties, Acta Biomater 169 (2023) 118–129.
[115] J. Castelein, C. Pamplona, R. Armstrong Junior, M. Vidal Dos Santos, I. Sack, R. Dierckx, C. Moers, R. Borra, Effects of kidney perfusion on renal stiffness and tissue fluidity measured with tomoelastography in an MRI-compatible ex vivo model. Front Bioeng, Biotechnol 11 (2023) 1236949.
[116] A.A. de Schellenberger, H. Tzschatzsch, B. Polchlopek, G. Bertalan, F. Schrank, K. Garczynska, P.A. Janmey, J. Braun, I. Sack, Sensitivity of multifrequency magnetic resonance elastography and diffusion-weighted imaging to cellular and stromal integrity of liver tissue, J Biomech 88 (2019) 201–208.
[117] H. Everwien, A. Ariza de Schellenberger, N. Haep, H. Tzschatzsch, J. Pratschke, I. M. Sauer, J. Braun, K.H. Hillebrandt, I. Sack, Magnetic resonance elastography quantification of the solid-to-fluid transition of liver tissue due to decellularization, J Mech Behav Biomed Mater 104 (2020) 103640.
[118] C.A. Hudert, H. Tzschatzsch, B. Rudolph, C. Loddenkemper, H.G. Holzhutter, L. Kalveram, S. Wiegand, J. Braun, I. Sack, J. Guo, How histopathologic changes in pediatric nonalcoholic fatty liver disease influence in vivo liver stiffness, Acta Biomaterialia 123 (2021) 178–186.
[119] K.J. Parker, J. Ormachea, S.A. McAleavey, R.W. Wood, J.J. Carroll-Nellenback, R. K. Miller, Shear wave dispersion behaviors of soft, vascularized tissues from the microchannel flow model, Phys Med Biol 61 (13) (2016) 4890–4903.
[120] M. Yin, K.J. Glaser, A. Manduca, T. Mounajjed, H. Malhi, D.A. Simonetto, R. Wang, L. Yang, S.A. Mao, J.M. Glorioso, F.M. Elgilani, C.J. Ward, P.C. Harris, S. L. Nyberg, V.H. Shah, R.L. Ehman, Distinguishing between Hepatic Inflammation and Fibrosis with MR Elastography, Radiology 284 (3) (2017) 694–705.
[121] M. Yin, A. Kolipaka, D.A. Woodrum, K.J. Glaser, A.J. Romano, A. Manduca, J. A. Talwalkar, P.A. Araoz, K.P. McGee, N.S. Anavekar, R.L. Ehman, Hepatic and splenic stiffness augmentation assessed with MR elastography in an in vivo porcine portal hypertension model, J Magn Reson Imaging 38 (4) (2013) 809–815.
[122] S. Ipek-Ugay, H. Tzschatzsch, J. Braun, T. Fischer, I. Sack, Physiologic Reduction of Hepatic Venous Blood Flow by the Valsalva Maneuver Decreases Liver Stiffness, Journal of Ultrasound in Medicine 36 (7) (2017) 1305–1311.
[123] T. Meyer, H. Tzschatzsch, B. Wellge, I. Sack, T. Kroncke, A. Martl, Valsalva Maneuver Decreases Liver and Spleen Stiffness Measured by Time-Harmonic Ultrasound Elastography, Front Bioeng Biotechnol 10 (2022) 886363.
[124] C.D.G. Hines, M.J. Lindstrom, A.K. Varma, S.B. Reeder, Effects of Postprandial State and Mesenteric Blood Flow on the Repeatability of MR Elastography in Asymptomatic Subjects, Journal of Magnetic Resonance Imaging 33 (1) (2011) 239–244.
[125] M. Yin, J.A. Talwalkar, K.J. Glaser, S.K. Venkatesh, J. Chen, A. Manduca, R. L. Ehman, Dynamic postprandial hepatic stiffness augmentation assessed with MR elastography in patients with chronic liver disease, AJR Am J Roentgenol 197 (1) (2011) 64–70.
[126] S. Ipek-Ugay, H. Tzschatzsch, C. Hudert, S.R. Marticorena Garcia, T. Fischer, J. Braun, C. Althoff, I. Sack, Time Harmonic Elastography Reveals Sensitivity of Liver Stiffness to Water Ingestion, Ultrasound Med Biol 42 (6) (2016) 1289–1294.
[127] Y. Wang, J. Zhou, H. Lin, H. Wang, I. Sack, J. Guo, F. Yan, R. Li, Viscoelastic parameters derived from multifrequency MR elastography for depicting hepatic fibrosis and inflammation in chronic viral hepatitis, Insights Imaging 15 (1) (2024) 91.
[128] Y. Shi, Y.F. Qi, G.Y. Lan, Q. Wu, B. Ma, X.Y. Zhang, R.Y. Ji, Y.J. Ma, Y. Hong, Three-dimensional MR Elastography Depicts Liver Inflammation, Fibrosis, and Portal Hypertension in Chronic Hepatitis B or C, Radiology 301 (1) (2021) 154–162.
[129] G. Bertalan, C. Klein, S. Schreyer, B. Steiner, B. Kreft, H. Tzschatzsch, A.A. de Schellenberger, M. Nieminen-Kelha, J. Braun, J. Guo, I. Sack, Biomechanical properties of the hypoxic and dying brain quantified by magnetic resonance elastography, Acta Biomater 101 (2020) 395–402.
[130] S. Hetzer, F. Dittmann, K. Bormann, S. Hirsch, A. Lipp, D.J. Wang, J. Braun, I. Sack, Hypercapnia increases brain viscoelasticity, J Cereb Blood Flow Metab 39 (12) (2019) 2445–2455.
[131] B. Kreft, H. Tzschätzsch, F. Schrank, J. Bergs, K.J. Streitberger, S. Wäldchen, S. Hetzer, J. Braun, I. Sack, Time-Resolved Response of Cerebral Stiffness to Hypercapnia in Humans, Ultrasound Med Biol 46 (4) (2020) 936–943.
[132] A. Hatt, S. Cheng, K. Tan, R. Sinkus, L.E. Bilston, MR Elastography Can Be Used to Measure Brain Stiffness Changes as a Result of Altered Cranial Venous Drainage During Jugular Compression, AJNR Am J Neuroradiol 36 (10) (2015) 1971–1977.
[133] P.S. Lan, K.J. Glaser, R.L. Ehman, G.H. Glover, Imaging brain function with simultaneous BOLD and viscoelasticity contrast: fMRI/fMRE, Neuroimage 211 (2020) 116592.
[134] R. Forouhandehpour, M. Bernier, G. Gilbert, R. Butler, K. Whittingstall, E. Van Houten, Cerebral stiffness changes during visual stimulation: Differential physiological mechanisms characterized by opposing mechanical effects, Neuroimage: Reports 1 (2) (2021) 100014.
[135] A. Arani, H.K. Min, N. Fattahi, N.M. Wetjen, J.D. Trzasko, A. Manduca, C. R. Jack Jr., K.H. Lee, R.L. Ehman, J. Huston 3rd., Acute pressure changes in the brain are correlated with MR elastography stiffness measurements: initial feasibility in an in vivo large animal model, Magn Reson Med 79 (2) (2018) 1043–1051.
[136] B. Kreft, H. Tzschatzsch, M. Shahryari, P. Haffner, J. Braun, I. Sack, K. J. Streitberger, Noninvasive Detection of Intracranial Hypertension by Novel Ultrasound Time-Harmonic Elastography, Invest Radiol 57 (2) (2022) 77–84.
[137] T. Meyer, B. Kreft, J. Bergs, E. Antes, M.S. Anders, B. Wellge, J. Braun, M. Doyley, H. Tzschatzsch, I. Sack, Stiffness pulsation of the human brain detected by non-invasive time-harmonic elastography, Front Bioeng Biotechnol 11 (2023) 1140734.
[138] B. Kreft, J. Bergs, M. Shahryari, L.A. Danyel, S. Hetzer, J. Braun, I. Sack, H. Tzschatzsch, Cerebral Ultrasound Time-Harmonic Elastography Reveals Softening of the Human Brain Due to Dehydration, Front Physiol 11 (2020) 616984.
[139] G. Bertalan, P. Boehm-Sturm, S. Schreyer, A.S. Morr, B. Steiner, H. Tzschatzsch, J. Braun, J. Guo, I. Sack, The influence of body temperature on tissue stiffness, blood perfusion, and water diffusion in the mouse brain, Acta Biomater 96 (2019) 412–420.
[140] K.J. Streitberger, M. Reiss-Zimmermann, F.B. Freimann, S. Bayerl, J. Guo, F. Arlt, J. Wuerfel, J. Braun, K.T. Hoffmann, I. Sack, High-resolution mechanical imaging of glioblastoma by multifrequency magnetic resonance elastography, PLoS One 9 (10) (2014) e110588.
[141] G.R. Ge, J.P. Rolland, W. Song, M. Nedergaard, K.J. Parker, Fluid compartments influence elastography of the aging mouse brain, Phys Med Biol 68 (9) (2023).
[142] Y. Shi, L. Cang, X. Zhang, X. Cai, X. Wang, R. Ji, M. Wang, Y. Hong, The use of magnetic resonance elastography in differentiating autoimmune pancreatitis from pancreatic ductal adenocarcinoma: A preliminary study, Eur J Radiol 108 (2018) 13–20.
[143] L. Zhu, J. Guo, Z. Jin, H. Xue, M. Dai, W. Zhang, Z. Sun, J. Xu, S.R. Marticorena Garcia, P. Asbach, B. Hamm, I. Sack, Distinguishing pancreatic cancer and autoimmune pancreatitis with in vivo tomoelastography, Eur Radiol 31 (5) (2021) 3366–3374.
[144] R. Reiter, F.N. Loch, C. Kamphues, C. Bayerl, S.R. Marticorena Garcia, B. Siegmund, A.A. Kuhl, B. Hamm, J. Braun, I. Sack, P. Asbach, Feasibility of Intestinal MR Elastography in Inflammatory Bowel Disease, J Magn Reson Imaging (2021).
[145] S.R. Marticorena Garcia, B. Hamm, I. Sack, Tomoelastography for non-invasive detection and treatment monitoring in acute appendicitis, BMJ Case Rep 12 (8) (2019).
[146] S.T. Lang, J. Guo, A. Bruns, M. Durr, J. Braun, B. Hamm, I. Sack, S.R. Marticorena Garcia, Multiparametric Quantitative MRI for the Detection of IgA Nephropathy Using Tomoelastography, DWI, and BOLD Imaging, Invest Radiol 54 (10) (2019) 669–674.
[147] M. Grossmann, H. Tzschatzsch, S.T. Lang, J. Guo, A. Bruns, M. Durr, B.F. Hoyer, U. Grittner, M. Lerchbaumer, M. Nguyen Trong, M. Schultz, B. Hamm, J. Braun, I. Sack, S.R. Marticorena Garcia, US Time-Harmonic Elastography for the Early Detection of Glomerulonephritis, Radiology 292 (3) (2019) 676–684.
[148] S.R. Marticorena Garcia, T. Fischer, M. Durr, E. Gultekin, J. Braun, I. Sack, J. Guo, Multifrequency Magnetic Resonance Elastography for the Assessment of Renal Allograft Function, Invest Radiol 51 (9) (2016) 591–595.
[149] S.R. Marticorena Garcia, M. Grossmann, A. Bruns, M. Durr, H. Tzschatzsch, B. Hamm, J. Braun, I. Sack, J. Guo, Tomoelastography Paired With T2* Magnetic Resonance Imaging Detects Lupus Nephritis With Normal Renal Function, Invest Radiol 54 (2) (2019) 89–97.
[150] M. Yin, K.J. Glaser, J.A. Talwalkar, J. Chen, A. Manduca, R.L. Ehman, Hepatic MR Elastography: Clinical Performance in a Series of 1377 Consecutive Examinations, Radiology 278 (1) (2016) 114–124.

[151] M. Yin, J. Woollard, X. Wang, V.E. Torres, P.C. Harris, C.J. Ward, K.J. Glaser, A. Manduca, R.L. Ehman, Quantitative assessment of hepatic fibrosis in an animal model with magnetic resonance elastography, Magn Reson Med 58 (2) (2007) 346–353.
[152] P. Kennedy, M. Wagner, L. Castera, C.W. Hong, C.L. Johnson, C.B. Sirlin, B. Taouli, Quantitative Elastography Methods in Liver Disease: Current Evidence and Future Directions, Radiology 286 (3) (2018) 738–763.
[153] P. Asbach, D. Klatt, B. Schlosser, M. Biermer, M. Muche, A. Rieger, C. Loddenkemper, R. Somasundaram, T. Berg, B. Hamm, J. Braun, I. Sack, Viscoelasticity-based Staging of Hepatic Fibrosis with Multifrequency MR Elastography, Radiology 257 (1) (2010) 80–86.
[154] C.A. Hudert, H. Tzschatzsch, B. Rudolph, H. Blaker, C. Loddenkemper, H. P. Muller, S. Henning, P. Bufler, B. Hamm, J. Braun, H.G. Holzhutter, S. Wiegand, I. Sack, J. Guo, Tomoelastography for the Evaluation of Pediatric Nonalcoholic Fatty Liver Disease, Invest Radiol 54 (4) (2019) 198–203.
[155] R. Reiter, H. Tzschatzsch, F. Schwahofer, M. Haas, C. Bayerl, M. Muche, D. Klatt, S. Majumdar, M. Uyanik, B. Hamm, J. Braun, I. Sack, P. Asbach, Diagnostic performance of tomoelastography of the liver and spleen for staging hepatic fibrosis, Eur Radiol 30 (3) (2020) 1719–1729.
[156] Y. Takahashi, T. Fukusato, Histopathology of nonalcoholic fatty liver disease/ nonalcoholic steatohepatitis, World Journal of Gastroenterology 20 (42) (2014) 15539–15548.
[157] Y. Iwakiri, V. Shah, D.C. Rockey, Vascular pathobiology in chronic liver disease and cirrhosis - Current status and future directions, Journal of Hepatology 61 (4) (2014) 912–924.
[158] F. Sauer, L. Oswald, A. Ariza de Schellenberger, H. Tzschätzsch, F. Schrank, T. Fischer, J. Braun, C.T. Mierke, R. Valiullin, I. Sack, J.A. Käs, Collagen networks determine viscoelastic properties of connective tissues yet do not hinder diffusion of the aqueous solvent, Soft Matter 15 (14) (2019) 3055–3064.
[159] R.V. Silva, A.S. Morr, H. Herthum, S.P. Koch, S. Mueller, C.S. Batzdorf, G. Bertalan, T. Meyer, H. Tzschatzsch, A.A. Kuhl, P. Boehm-Sturm, J. Braun, M. Scheel, F. Paul, C. Infante-Duarte, I. Sack, Cortical matrix remodeling as a hallmark of relapsing-remitting neuroinflammation in MR elastography and quantitative MRI, Acta Neuropathol 147 (1) (2024) 8.
[160] D. Vestweber, How leukocytes cross the vascular endothelium, Nat Rev Immunol 15 (11) (2015) 692–704.
[161] M. Shahryari, S. Keller, D. Meierhofer, I. Wallach, Y. Safraou, J. Guo, S. R. Marticorena Garcia, J. Braun, M.R. Makowski, I. Sack, N. Berndt, On the relationship between metabolic capacities and in vivo viscoelastic properties of the liver, Front Bioeng Biotechnol 10 (2023) 1042711.
[162] J.M. Liefhebber, C.V. Hague, Q. Zhang, M.J. Wakelam, J. McLauchlan, Modulation of triglyceride and cholesterol ester synthesis impairs assembly of infectious hepatitis C virus, J Biol Chem 289 (31) (2014) 21276–21288.
[163] M. Duerr, E.V. Schrezenmeier, L.J. Lehner, L. Bergfeld, P. Glander, S.R.M. Garcia, C.E. Althoff, I. Sack, S. Brakemeier, K.U. Eckardt, K. Budde, F. Halleck, A prospective study of daclatasvir and sofosbuvir in chronic HCV-infected kidney transplant recipients, Bmc Nephrology 20 (2019).
[164] S.R. Marticorena Garcia, C.E. Althoff, M. Durr, F. Halleck, K. Budde, U. Grittner, C. Burkhardt, K. Johrens, J. Braun, T. Fischer, B. Hamm, I. Sack, J. Guo, Tomoelastography for Longitudinal Monitoring of Viscoelasticity Changes in the Liver and in Renal Allografts after Direct-Acting Antiviral Treatment in 15 Kidney Transplant Recipients with Chronic HCV Infection, J Clin Med 10 (3) (2021).
[165] S. Almutawakel, F. Halleck, M. Durr, U. Grittner, E. Schrezenmeier, K. Budde, C. E. Althoff, B. Hamm, I. Sack, T. Fischer, S.R. Marticorena Garcia, Shear Wave Elastography for Assessing Liver Stiffness in HCV-Infected Kidney Transplant Recipients after Direct-Acting Antiviral Treatment: A Comparative Study with Magnetic Resonance Elastography, J Clin Med 12 (24) (2023).
[166] S. Mueller, G. Millonig, L. Sarovska, S. Friedrich, F.M. Reimann, M. Pritsch, S. Eisele, F. Stickel, T. Longerich, P. Schirmacher, H.K. Seitz, Increased liver stiffness in alcoholic liver disease: differentiating fibrosis from steatohepatitis, World J Gastroenterol 16 (8) (2010) 966–972.
[167] R.A. Egnatchik, A.K. Leamy, S.A. Sacco, Y.E. Cheah, M. Shiota, J.D. Young, Glutamate-oxaloacetate transaminase activity promotes palmitate lipotoxicity in rat hepatocytes by enhancing anaplerosis and citric acid cycle flux, J Biol Chem 294 (9) (2019) 3081–3090.
[168] F.J. Ammon, A. Kohlhaas, O. Elshaarawy, J. Mueller, T. Bruckner, C. Sohn, G. Fluhr, H. Fluhr, S. Mueller, Liver stiffness reversibly increases during pregnancy and independently predicts preeclampsia, World J Gastroenterol 24 (38) (2018) 4393–4402.
[169] K. Garczynska, H. Tzschatzsch, A.A. Kuhl, A.S. Morr, L. Lilaj, A. Hackel, E. Schellenberger, N. Berndt, H.G. Holzhutter, J. Braun, I. Sack, J. Guo, Changes in Liver Mechanical Properties and Water Diffusivity During Normal Pregnancy Are Driven by Cellular Hypertrophy, Front Physiol 11 (2020) 605205.
[170] J. Nees, F.J. Ammon, J. Mueller, H. Fluhr, S. Mueller, Liver stiffness in pregnant women with intrahepatic cholestasis of pregnancy: A case control study, World J Hepatol 15 (7) (2023) 904–913.
[171] K.J. Streitberger, A. Fehlner, F. Pache, A. Lacheta, S. Papazoglou, J. Bellmann-Strobl, K. Ruprecht, A. Brandt, J. Braun, I. Sack, F. Paul, J. Wuerfel, Multifrequency magnetic resonance elastography of the brain reveals tissue degeneration in neuromyelitis optica spectrum disorder, European Radiology 27 (5) (2017) 2206–2215.
[172] K.J. Streitberger, I. Sack, D. Krefting, C. Pfuller, J. Braun, F. Paul, J. Wuerfel, Brain viscoelasticity alteration in chronic-progressive multiple sclerosis, PLoS One 7 (1) (2012) e29888.
[173] J. Wuerfel, F. Paul, B. Beierbach, U. Hamhaber, D. Klatt, S. Papazoglou, F. Zipp, P. Martus, J. Braun, I. Sack, MR-elastography reveals degradation of tissue integrity in multiple sclerosis, Neuroimage 49 (3) (2010) 2520–2525.
[174] A. Fehlner, J.R. Behrens, K.J. Streitberger, S. Papazoglou, J. Braun, J. Bellmann-Strobl, K. Ruprecht, F. Paul, J. Wurfel, I. Sack, Higher-resolution MR elastography reveals early mechanical signatures of neuroinflammation in patients with clinically isolated syndrome, J Magn Reson Imaging 44 (1) (2016) 51–58.
[175] J.M. Millward, J. Guo, D. Berndt, J. Braun, I. Sack, C. Infante-Duarte, Tissue structure and inflammatory processes shape viscoelastic properties of the mouse brain, NMR Biomed 28 (7) (2015) 831–839.
[176] S. Wang, J.M. Millward, L. Hanke-Vela, B. Malla, K. Pilch, A. Gil-Infante, S. Waiczies, S. Mueller, P. Boehm-Sturm, J. Guo, I. Sack, C. Infante-Duarte, MR Elastography-Based Assessment of Matrix Remodeling at Lesion Sites Associated With Clinical Severity in a Model of Multiple Sclerosis, Front Neurol 10 (2019) 1382.
[177] K. Riek, J.M. Millward, I. Hamann, S. Mueller, C.F. Pfueller, F. Paul, J. Braun, C. Infante-Duarte, I. Sack, Magnetic resonance elastography reveals altered brain viscoelasticity in experimental autoimmune encephalomyelitis, NeuroImage: Clinical 1 (1) (2012) 81–90.
[178] K. Schregel, E. Wuerfel, P. Garteiser, I. Gemeinhardt, T. Prozorovski, O. Aktas, H. Merz, D. Petersen, J. Wuerfel, R. Sinkus, Demyelination reduces brain parenchymal stiffness quantified in vivo by magnetic resonance elastography, Proc Natl Acad Sci U S A 109 (17) (2012) 6650–6655.
[179] L.M. Solamen, S.W. Gordon-Wylie, M.D. McGarry, J.B. Weaver, K.D. Paulsen, Phantom evaluations of low frequency MR elastography, Phys Med Biol 64 (6) (2019) 065010.
[180] R. Reiter, M. Shahryari, H. Tzschatzsch, M. Haas, C. Bayerl, B. Siegmund, B. Hamm, P. Asbach, J. Braun, I. Sack, Influence of fibrosis progression on the viscous properties of in vivo liver tissue elucidated by shear wave dispersion in multifrequency MR elastography, J Mech Behav Biomed Mater 121 (2021) 104645.
[181] K.M. Pepin, C.L. Welle, F.F. Guglielmo, J.R. Dillman, S.K. Venkatesh, Magnetic resonance elastography of the liver: everything you need to know to get started, Abdominal Radiology 47 (1) (2022) 94–114.
[182] H. Herthum, S. Hetzer, B. Kreft, H. Tzschatzsch, M. Shahryari, T. Meyer, S. Gorner, H. Neubauer, J. Guo, J. Braun, I. Sack, Cerebral tomoelastography based on multifrequency MR elastography in two and three dimensions, Front Bioeng Biotechnol 10 (2022) 1056131.